iScience

CellPress
OPEN ACCESS

Article

A Viral Toolbox of Genetically Encoded Fluorescent Synaptic Tags

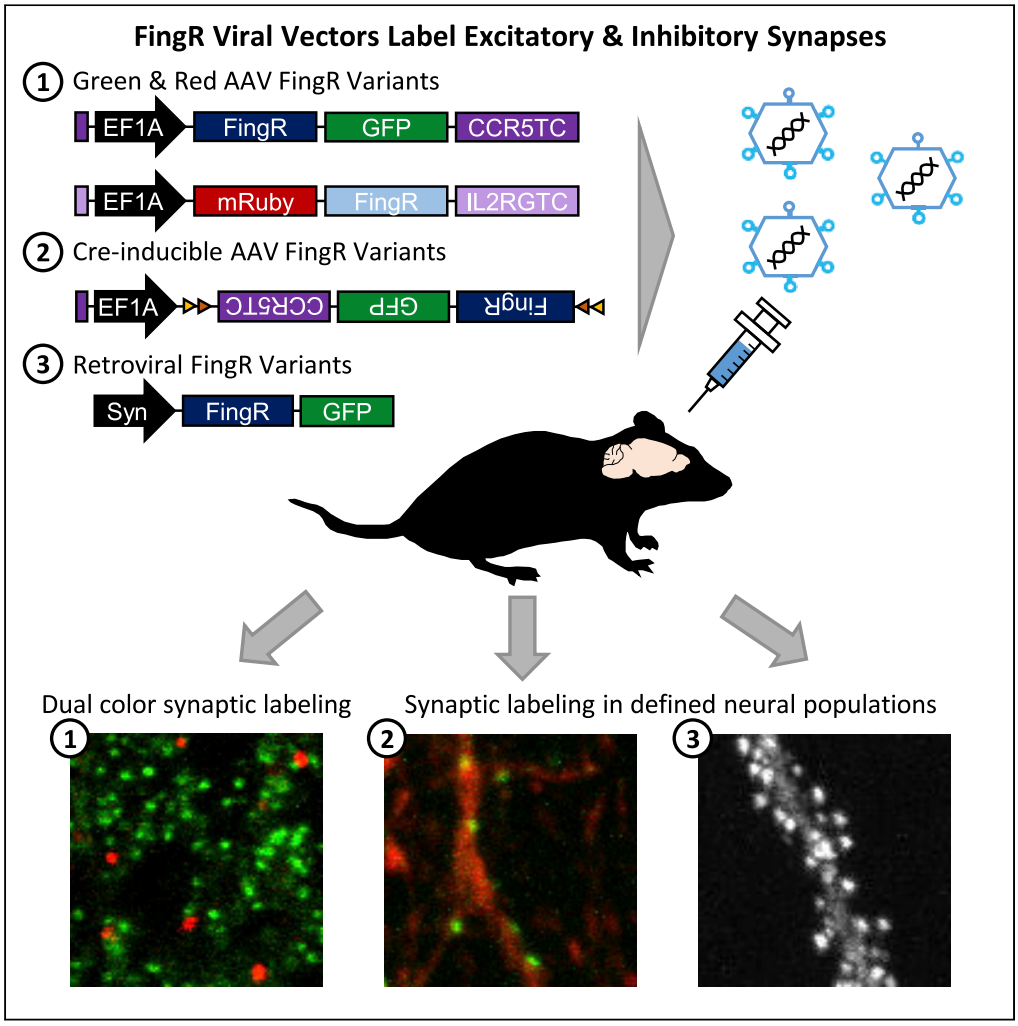

Seth Bensussen, Sneha Shankar, Kimberley H. Ching, ..., Connor Beck, Heng-Ye Man, Xue Han

xuehan@bu.edu

HIGHLIGHTS

AAV FingR vectors globally label excitatory or inhibitory synapses in neurons

AAV FingRs dually label excitatory and inhibitory synapses in the same neuron

Cre-inducible FingR AAV vectors label synapses in defined neuron populations

Retroviral FingR vectors allow tracking of synaptic development in newborn neurons

Bensussen et al., iScience *23*, 101330
July 24, 2020
https://doi.org/10.1016/j.isci.2020.101330

iScience

CellPress
OPEN ACCESS

Article

A Viral Toolbox of Genetically Encoded Fluorescent Synaptic Tags

Seth Bensussen,[1] Sneha Shankar,[1] Kimberley H. Ching,[1] Dana Zemel,[1] Tina L. Ta,[1] Rebecca A. Mount,[1] Sanaya N. Shroff,[1] Howard J. Gritton,[1] Pierre Fabris,[1] Hannah Vanbenschoten,[1] Connor Beck,[1] Heng-Ye Man,[2] and Xue Han[1,3,*]

SUMMARY

Fibronectin intrabodies generated with mRNA display (FingRs) are a recently developed tool for labeling excitatory or inhibitory synapses, with the benefit of not altering endogenous synaptic protein expression levels or synaptic transmission. Here, we generated a viral vector FingR toolbox that allows for multi-color, neuron-type-specific labeling of excitatory or inhibitory synapses in multiple brain regions. We screened various fluorophores, FingR fusion configurations, and transcriptional control regulations in adeno-associated virus (AAV) and retrovirus vector designs. We report the development of a red FingR variant and demonstrated dual labeling of excitatory and inhibitory synapses in the same cells. Furthermore, we developed cre-inducible FingR AAV variants and demonstrated their utility, finding that the density of inhibitory synapses in aspiny striatal cholinergic interneurons remained unchanged in response to dopamine depletion. Finally, we generated FingR retroviral vectors, which enabled us to track the development of excitatory and inhibitory synapses in hippocampal adult-born granule cells.

INTRODUCTION

Electrical and chemical signaling at the synapses between neurons is essential for neural computation. Tools that allow for precise synaptic labeling provide important information regarding connectivity and plasticity and are essential for mapping and understanding neural circuits. Traditional immunohistochemistry methods use antibodies developed against individual endogenous synaptic proteins, which requires fixation of tissue and thus prevents the visualization of live tissues. At the synaptic level, traditional immunohistochemistry non-selectively labels the dense array of synaptic puncta, making it difficult to distinguish or assign particular synaptic puncta to the specific cell from which each synapse originates. Staining for synaptic proteins in particular can be challenging because it is often difficult for large antibodies to penetrate the dense packing of proteins at the postsynaptic density (Ryan and Grant, 2009; Sheng and Hoogenraad, 2007; Watanabe et al., 1998). Several methods have been developed to enhance antibody penetration, but these methods require optimization and often are unreliable (Watanabe et al., 1998).

Genetically encoded fluorescent proteins enable cell-type specific labeling of live or fixed tissue using cell-type specific promoters or recombinase systems (Sjulson et al., 2016). Because of the unique bouton-like structure of excitatory synapses, it is possible to use GFP expression to identify excitatory dendritic spines based on shape alone (Day et al., 2006; van Praag et al., 2002). However, this method fails to work for identifying inhibitory synapses that are generally present on the dendritic shaft, or for identifying excitatory synapses on aspiny neurons that do not form distinctive bouton-like structures (Chen et al., 2012; Kwon et al., 2018). Expressing exogenous synaptic proteins fused with fluorophores has been used to tag excitatory and inhibitory synapses, offering comparable spatial resolution as antibodies (Bosch et al., 2014; Cane et al., 2014; Chen et al., 2012; Meyer et al., 2014; Specht et al., 2013; Villa et al., 2016). However, exogenous overexpression of synaptic proteins has the potential to disturb synaptic physiology (El-Husseini et al., 2000). Although the use of transgenic mouse lines with fluorescent proteins fused to endogenous synaptic proteins remains a viable solution (Broadhead et al., 2016; Fortin et al., 2014; Masch et al., 2018; Zhu et al., 2018), the timelines for generating specific transgenic lines for each synapse type and fluorophore color of interest has limited such strategies.

[1]Department of Biomedical Engineering, Boston University, Boston, MA 02215, USA

[2]Department of Biology, Boston University, Boston, MA 02215, USA

[3]Lead Contact

*Correspondence: xuehan@bu.edu

https://doi.org/10.1016/j.isci.2020.101330

Recently, genetically encoded tools have been developed to map functional synapses or label excitatory or inhibitory synapses without modifying endogenous protein levels (Chen et al., 2014; Gross et al., 2013; Kim et al., 2011; Macpherson et al., 2015). In particular, fibronectin intrabodies generated with mRNA display (FingRs) developed against synaptic proteins PSD95 and gephyrin present a method to fluorescently label excitatory and inhibitory synapses without disrupting endogenous proteins (Gross et al., 2013). PSD95 is a scaffolding protein at excitatory synapses, and gephyrin acts as a scaffolding protein at inhibitory synapses. The genetically encoded FingRs against PSD95 (PSD95.FingR) and against gephyrin (Gephyrin.FingR) bind to PSD95 and gephyrin, respectively, and act as intracellular antibodies in live and fixed neurons. To prevent overexpression of the FingRs, a transcriptional control system has been used to ensure that FingR expression levels matched those of the endogenous protein target (Gross et al., 2013). Because the FingRs bind to the endogenous synaptic proteins, they do not alter the expression levels of endogenous proteins. Furthermore, it has been shown that expression of PSD95.FingR and Gephyrin.FingR does not disrupt synaptic physiology (Gross et al., 2013). These proteins, when introduced through transfection or *in utero* electroporation, have been successfully used in neuron cultures, mouse brain slices, and live transgenic zebrafish (Gross et al., 2013; Kannan et al., 2016; Kwon et al., 2018; Sinnen et al., 2017; Walker et al., 2017). Although available in DNA plasmid form, there have been no viral vectors that allow FingRs to be easily used in the brain.

To enable broad application of FingR-based synaptic tagging strategies, we developed a set of PSD95.FingR and Gephyrin.FingR viral vectors. We generated FingR adeno-associated viruses (AAVs), with both strong constitutive and cre-inducible expression, for labeling of excitatory or inhibitory synapses in cortical and subcortical brain regions. We screened a number of red-shifted reporter FingRs with various configurations of red fluorescent proteins (RFP) and FingR fusions and identified that N-terminally fused FingRs retained synaptic targeting specificity. These red FingRs when packaged into AAV viral vectors can be used in conjunction with green FingRs for dual-color synaptic labeling globally, and in a cell-type-specific manner in cre-dependent transgenic mice. Furthermore, we explored the impact of transcriptional control in retroviral vector designs and discovered that the use of a transcriptional control element diminished FingR expression in retroviral vectors. We thus generated FingR retroviral vectors without transcriptional control, which allowed us to label excitatory and inhibitory synapses in adult-born granule cells and track the synaptic development of adult-born neurons throughout the maturation period. Overall, these FingR viral vectors will facilitate neuroscience studies mapping neural circuitry, tracking synaptic development, or studying plasticity, during normal and disease conditions.

RESULTS

Global Labeling of Excitatory and Inhibitory Synapses across Cortical and Subcortical Brain Regions

To enable broad application of FingR-based synaptic tagging strategies, we constructed AAV genomic vectors, AAV-EF1α-PSD95.FingR-GFP-CCR5TC and AAV-EF1α-Gephyrin.FingR-GFP-CCR5TC, expressing the PSD95.FingR and Gephyrin.FingR, respectively, under a strong elongation factor-1 alpha (EF1α) promoter and with the CCR5 transcriptional feedback regulator domain (CCR5TC) fused to the C terminus of the GFP (Figure 1A). The CCR5TC domain consists of a DNA sequence recognizing CCR5 zinc finger protein fused to a KRAB(A) transcriptional repressor domain as described previously (Gross et al., 2013). We then packaged AAV viral particles with AAV9 coat proteins, which exhibit excellent expression levels in the rodent central nervous system (Cearley and Wolfe, 2006; Foust et al., 2009; Gritton et al., 2019; Zincarelli et al., 2008). We injected both viral vectors separately into the cortex, striatum, and hippocampus of the mouse brain and analyzed the expression patterns in each brain region following histochemical processing of fixed brain sections 3 weeks post-injection. We detected strong GFP punctate expression patterns in all brain areas tested, along with labeled cell nuclei (Figures 1B–1G). The PSD95.FingR puncta density appeared higher than the Gephyrin.FingR density in all brain regions tested, consistent with previous observations of higher excitatory than inhibitory synaptic densities (Megıas et al., 2001; Tepper et al., 2007; Villa et al., 2016).

To verify the identity of the labeled puncta, we used traditional antibody staining and analyzed the co-localization patterns of immunofluorescence and GFP. We found strong co-localization between Gephyrin.-FingR-GFP and the gephyrin antibody in mouse brain slices (Figure 1I), where 69.1% ± 6.0% (mean ± standard deviation, n = 6 slices, from 4 mice) of the Gephyrin.FingR-GFP-positive puncta co-localized with gephyrin immunofluorescence (Figure 1J). As the PSD95 antibody has difficulty penetrating the postsynaptic density without optimized antigen retrieval methods (Fritschy et al., 1998), we examined the co-localization of PSD95.FingR-GFP with the excitatory post-synaptic marker Homer and pre-synaptic marker

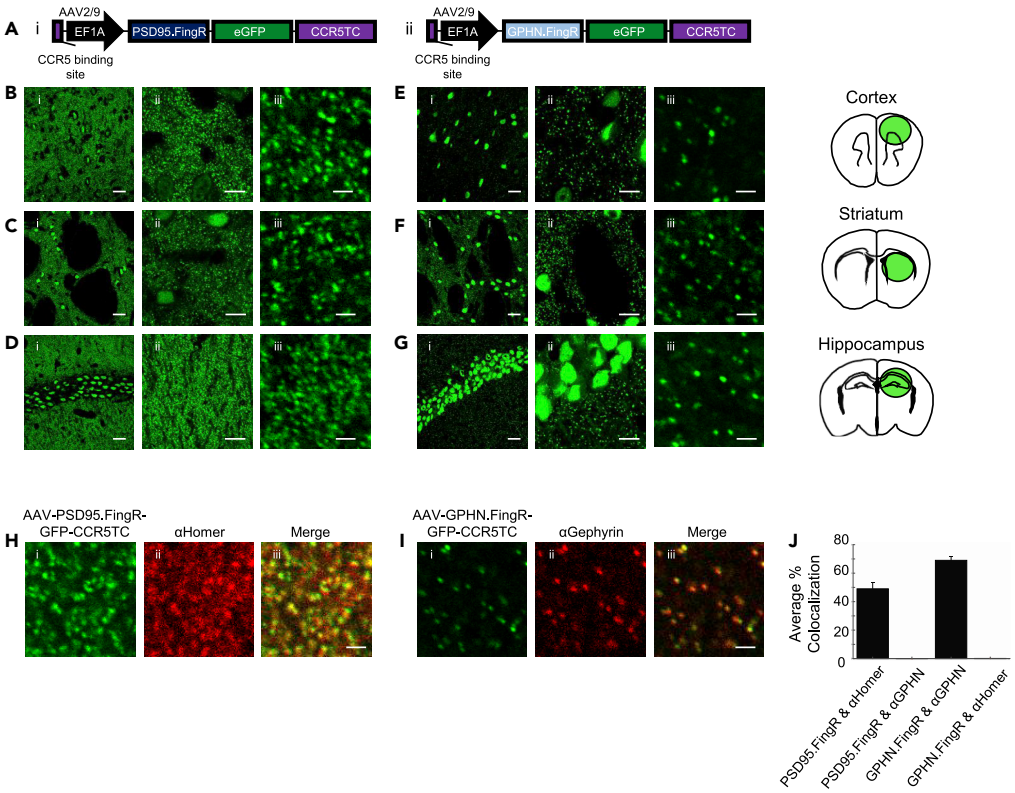

Figure 1. PSD95.FingR and Gephyrin.FingR AAVs Globally Label Excitatory and Inhibitory Synapses with Submicron Resolution

(A) DNA construct diagrams for (i) PSD95.FingR and (ii) Gephyrin.FingR (GPHN.FingR). Both constructs use the AAV2 transfer backbone and were packaged with the serotype 9 coat proteins. CCR5TC is the transcriptional repressor domain responsible for transcriptional control, which recognizes the CCR5 binding site upstream of the EF1α promoter to regulate the potential for overexpression of the FingR proteins.

(B–D) Representative images of PSD95.FingR expression in the motor cortex (B), striatum (C), and hippocampus (D) of mouse brain slices. Images shown at 60× (i), 60× with 4× zoom (ii), and 60× with 20× zoom (iii). Scale bars: 25μm in (i), 10 μm in (ii), and 2 μm in (iii).

(E–G) Representative images of Gephyrin.FingR expression in the motor cortex (E), striatum (F), and hippocampus (G) of mouse brain slices. Images shown at 60× (i), 60× with 4× zoom (ii), and 60× with 20× zoom (iii). Scale bars: 25 μm in (i), 10 μm in (ii), and 2 μm in (iii).

(H) Brain slices expressing PSD95.FingR (i), stained with a homer antibody (ii), and co-localization (iii). Scale bar, 2 μm.

(I) Brain slices expressing Gephyrin.FingR (i), stained with a gephyrin antibody (ii), and co-localization (iii). Scale bar, 2 μm.

(J) Quantification of co-localization between synapses labeled with PSD95.FingR, Homer antibody, GPHN.FingR, and gephyrin (GPHN) antibody. PSD95.FingR-labeled synapses co-localized with Homer antibody significantly more than with GPHN antibody, and GPHN.FingR-labeled synapses co-localized with gephyrin antibody significantly more than with Homer antibody (***$p < 0.001$, two-tailed t test).

Data represented as mean ± standard deviation. For additional data, see also Figures S1, S2, and S8.

Bassoon in brain slices and found strong co-localization (Figures 1H and S1) (Dani et al., 2010; Fukaya and Watanabe, 2000; Gutierrez-Mecinas et al., 2016). We found 49.0% ± 10.3% (mean ± standard deviation, n = 6 slices, from 4 mice) of the PSD.FingR-positive puncta co-localized with Homer immunofluorescence (Figure 1J), which is in line with previous findings (Sinnen et al., 2017). Furthermore, the PSD95.FingR expressed in neuron culture co-localized with a PSD95 antibody, and co-injection of AAV-EF1α-PSD95.FingR-GFP-CCR5TC and AAV-Syn-PSD95-mCherry showed co-localization in mouse brain slices, further confirming that the PSD95.FingR co-localizes with endogenous PSD95 (Figure S1). As a control, we assessed the co-localization between Gephyrin.FingR-GFP-positive puncta and Homer immunofluorescence, as well as between PSD95.FingR-GFP-positive puncta and gephyrin immunofluorescence and found 0.03% ± 0.02% and 0.11% ± 0.08% (mean ± standard deviation, n = 6 slices, from 2 to 3 mice) co-localization for these control combinations, respectively. Together, these results demonstrate that

AAV-EF1α-PSD95.FingR-GFP-CCR5TC and AAV-EF1α-Gephyrin.FingR-GFP-CCR5TC selectively labeled excitatory and inhibitory neurons, respectively, when injected in the mouse brain.

It is useful to note that expression of the AAV-Syn-PSD95.FingR-GFP-CCR5TC under a slightly weaker, but neuron-specific, synapsin promoter still displayed a punctate expression pattern in all three brain regions (Figure S2). We also generated FingR lentiviruses pseudotyped with vesicular stomatitis virus G protein (VSV-G) containing a calmodulin kinase II alpha (CamKIIa) promoter and found that these lentiviruses mediated weak expression in mouse brain slices (Figure S3). The lentivirus designed to express PSD95.FingR-GFP (lenti-CamKIIa-PSD95.FingR-GFP-CCR5TC) showed punctate expression patterns, whereas the lentivirus designed to express Gephyrin.FingR-mRuby2 (lenti-CamKIIa-Gephyrin.FingR-mRuby2-IL2RGTC) only showed expression in the nuclei of cells with no punctate patterns along the dendrites. Overall, the AAV-EF1A-PSD95.FingR-GFP-CCR5TC and AAV-EF1A-Gephyrin.FingR-GFP-CCR5TC viruses enable synaptic labeling in multiple brain regions while maintaining sub-micron spatial resolution.

Generation of a Red Gephyrin.FingR Variant that Enables Dual-Color Synaptic Labeling

We next designed a red FingR variant that can be used simultaneously with the green FingRs (Figure 1) to enable dual-color labeling of both excitatory and inhibitory synapses in the same neurons. Although dual-color synaptic labeling has been shown in neuron cultures and zebrafish, there has been no demonstration of two-color synaptic labeling in mammalian brain tissue using the FingR tags (Gross et al., 2013; Son et al., 2016). In general, red fluorescent proteins are dimmer, more susceptible to aggregation, and do not function as well in fusion proteins when compared with GFP (Bindels et al., 2017). To address this, we selected a bright monomeric red fluorescent protein mScarlet, which exhibits the highest quantum yield and has shown excellent performance as a fusion tag (Bindels et al., 2017).

We generated the mScarlet variants of the Gephyrin.FingR using the IL2RG transcriptional control system that is orthogonal to the CCR5 transcriptional control system (Gross et al., 2013; Son et al., 2016). Because protein fusion could alter FingR binding to its protein target and mScarlet fluorescence levels, we first examined different fusion protein configurations by fusing mScarlet either to the N terminal or to the C terminal of Gephyrin.FingR (Figure 2A). Interestingly, we found that the N-terminally fused mScarlet-Gephyrin.FingR yielded a much more punctate expression pattern than the C-terminally fused Gephyrin.FingR-mScarlet (Figures 2B and 2C). This suggests that FingRs are sensitive to protein tagging, and that the location of the fluorophore could impact FingR expression levels and co-localization with endogenous proteins.

We then further screened other red fluorescent proteins, mRuby2 and mCherry, fused to the N terminal of Gephyrin.FingR based on our findings described earlier (Figure 2A) (Lam et al., 2012; Shaner et al., 2004). In neuron cultures, Gephyrin.FingR-mScarlet, mScarlet-Gephyrin.FingR, and mRuby2-Gephyrin.FingR co-localized with the immunofluorescence of the gephyrin antibody (70.3% ± 4.4%, 69.2% ± 2.5%, and 76.4 ± 3.4% respectively, from 5 fields of view (FOVs) each, Figures 2B–2D), similar to that achieved by the green gephyrin.FingR-GFP (Figure 1J). However, mCherry-Gephyrin.FingR largely formed aggregates and showed little expression at the synapses (Figure 2E). The poor expression of mCherry-Gephyrin.FingR is consistent with previous findings that mCherry aggregates when expressed in neurons (Lichtman et al., 2013). Together, these results demonstrate that the variants with mScarlet and mRuby2 fused to the N terminal of the Gephyrin.FingR retain the functionality of the FingRs and allow inhibitory synaptic labeling with these red fluorescent proteins.

To demonstrate the use of dual-color synaptic labeling, we co-injected AAV-EF1A-PSD95.FingR-GFP-CCR5TC with the functional red Gephyrin.FingR variant AAV-EF1A-mRuby2-Gephyrin.FingR-IL2RGTC into the mouse brain (Figure 2F). This way, we could determine not only if the red Gephyrin.FingR properly labels inhibitory synapses but also if it interacts with the PSD95.FingR-GFP. Similar to the neuron culture results, AAV-EF1A-mRuby2-Gephyrin.FingR-IL2RGTC exhibited a punctate expression pattern in mouse brain sections when co-expressed with AAV-EF1A-PSD95.FingR-GFP-CCR5TC, and these two FingRs labeled non-co-localized synaptic puncta (1.3% ± 0.3% co-localization, from 5 FOVs, Figures 2G–2J). Further validation with the homer and gephyrin antibodies confirmed that PSD95.FingR-GFP labeled excitatory synapses (67.0% ± 3.4% co-localization with homer antibody, and 1.0% ± 0.4% co-localization with gephyrin antibody, from 5 FOVs each), whereas mRuby-gephyrin.FingR labeled inhibitory synapses (76.6% ± 5.2% co-localization with gephyrin antibody and 0% ± 0% co-localization with homer antibody, from 5 FOVs each) (Figure S5). Similarly, AAV-EF1A-mScarlet-Gephyrin.FingR-IL2RGTC and AAV-EF1A-

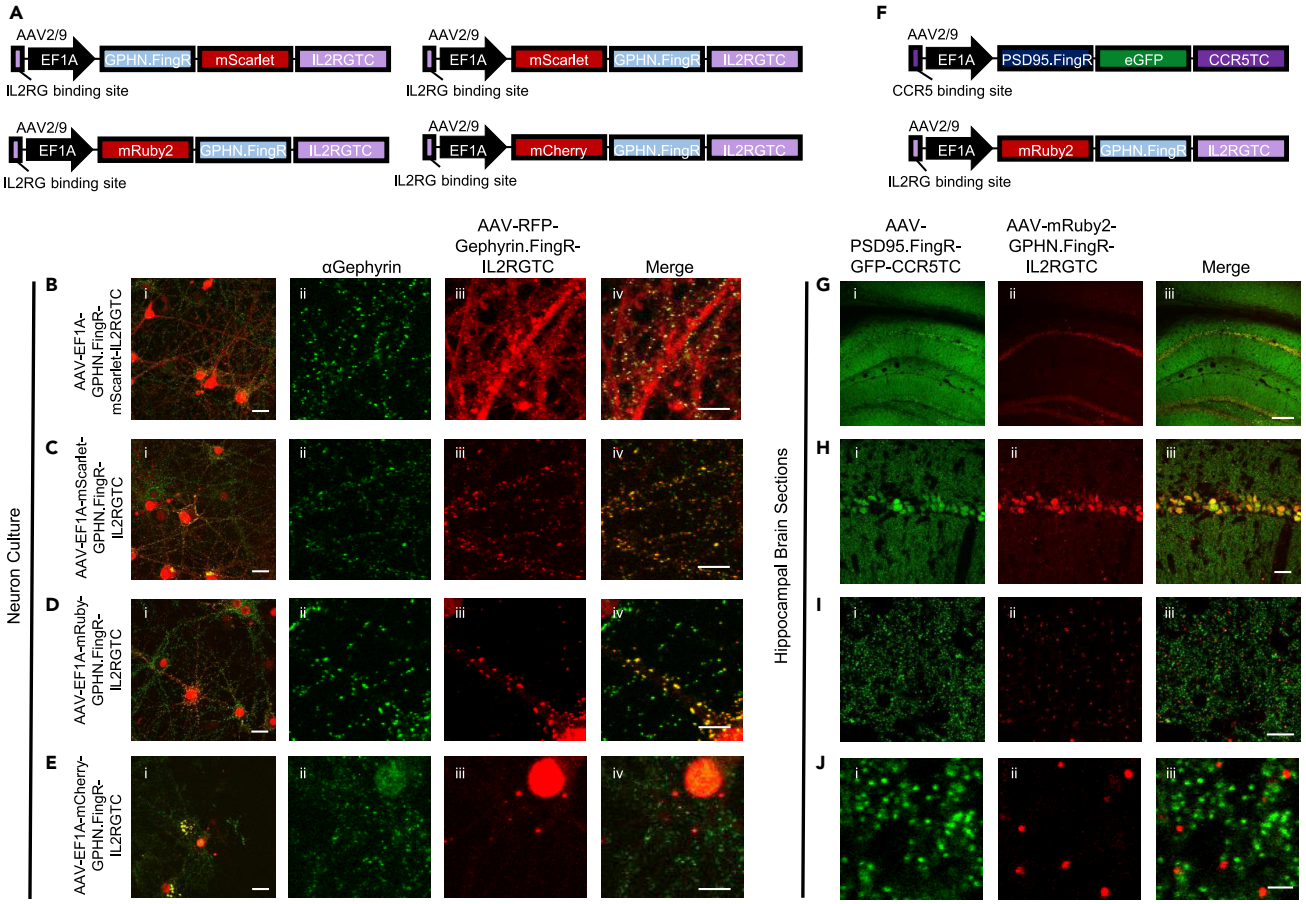

Figure 2. Optimization of a Red Gephyrin.FingR AAV Enables Dual Synaptic Labeling of Excitatory and Inhibitory Synapses

(A) DNA construct diagrams for the red Gephyrin AAV variants tested. The IL2RGTC domain acts orthogonally to the CCR5TC domain. The IL2RGTC domain is a transcriptional repressor that recognizes the IL2RG binding site upstream of the EF1A promoter to prevent overexpression of the FingR proteins.

(B–E) Representative images of Gephyrin.FingR-mScarlet (B), mScarlet-Gephyrin.FingR (C), mRuby2-Gephyrin.FingR (D), and mCherry-Gephyrin.FingR (E) infected neurons and stained with the gephyrin antibody (i). Zoomed-in images showing synapses stained with the gephyrin antibody (ii), RFP-Gephyrin.FingR expression (iii), and co-localization between RFP and the antibody (iv). Scale bars: 25 μm in (i) and 10 μm in (ii, iii, and iv).

(F) DNA construct diagrams for the co-injected viruses PSD95.FingR-GFP (label excitatory synapses in green) and mRuby2-Gephyrin.FingR (label inhibitory synapses in red).

(G–J) Representative images of the expression patterns of the co-injected PSD95.FingR-GFP AAV (i) and mRuby2-Gephyrin.FingR AAV (ii) and their merge (iii) in mouse hippocampal brain slices shown at 10× (G), 60× (H), 60× with 4× zoom (I), and 60× with 20× zoom (J). Note the co-localization of cell bodies labeled and non-co-localized punctate synaptic expression, as expected.

Scale bars, 200 μm in (G), 25 μm in (H), 10 μm in (I), and 2 μm in (J). For additional data, see also Figures S4 and S5.

PSD95.FingR-GFP-CCR5TC labeled non-co-localized synaptic puncta in the mouse brain (0% ± 0% co-localization, from 5 FOVs, Figure S4). Thus, AAV-EF1A-PSD95.FingR-GFP-CCR5TC and AAV-EF1A-mRuby2-Gephyrin.FingR-IL2RGTC represent a pair of FingR tags that can be used orthogonally to label both excitatory and inhibitory synapses in the same brain tissue.

Retroviral Vectors Allow Labeling of Excitatory and Inhibitory Synapses in Hippocampal Adult-Born Granule Cells

Although most neurons are non-dividing, adult neurogenesis occurs in the subventricular and subgranular zones of mammalian brains. Neurons born in the subgranular zone develop into granule cells and functionally integrate into the dentate gyrus of the hippocampus (Toni et al., 2007; van Praag et al., 2002; Zhao et al., 2006). Several studies have demonstrated important functions of adult neurogenesis in hippocampal-dependent behavioral tasks (Danielson et al., 2016; Nakashiba et al., 2012; Zhuo et al., 2016). Interestingly, adult-born granule cells undergo a critical period about 1 to 2 months after cell birth where they exhibit increased excitability and display heightened plasticity (Ge et al., 2007; Schmidt-Hieber et al., 2004).

Adult-born hippocampal granule cells have been shown to first form GABAergic synapses along the dendrites, starting within a week after birth, whereas excitatory synapses and dendritic spines do not form until 2 weeks after birth in mice (Toni and Sultan, 2011). Peak spine formation occurs during the third week after birth, coinciding with the observed critical development window important for their function (Toni and Sultan, 2011). Although several studies have outlined the detailed timeline for synaptic development in adult-born granule cells using electrophysiology and cell morphology, it remains difficult to study the synapses on newborn cells in isolation. Although antibodies exist for labeling excitatory and inhibitory synapses, it is impossible to distinguish synapses formed onto adult-born granule cells from those onto mature dentate granule cells, even if the adult-born cells are labeled with fluorescent proteins. Genetically encoded FingR synaptic tags can overcome these issues by only labeling synapses within adult-born neurons.

To express the PSD95.FingR and Gephyrin.FingR in adult-born neurons, we used a murine stem cell virus (MSCV) retroviral expression system with a synapsin promoter that has been shown to mediate strong and specific gene expression in adult-born dentate granule cells born within a day of viral injection (Zhuo et al., 2016). The negative feedback transcriptional control of the FingR proteins ensures that transgene expression matches the levels of endogenous proteins, whereas our lentivirus mediated low levels of FingR expression as demonstrated in Figure S3. As lentivirus pseudotyped with VSV-G is known to have similar or slightly higher transduction efficiency than MSCV retrovirus, we constructed retroviral vectors containing synapsin-driven FingR-GFP expression, with and without transcriptional control. Upon initial testing in HEK cells, we could not detect any GFP fluorescence in the transcriptionally regulated retrovirus FingR variants (Figure S6). Thus, we injected retrovirus MSCV-Syn-PSD95.FingR-GFP and MSCV-Syn-Gephyrin.FingR-GFP, without transcriptional control, and an MSCV-Syn-GFP control virus into the dentate gyrus of adult mice, and analyzed synaptic puncta 4 weeks after the viral injections (Figures 3A and 3B). We found that MSCV-Syn-FingR-GFP-labeled neurons exhibited a distinct and punctate GFP expression pattern (Figure 3B) and also showed weak fluorescence in the dendrites, which can be used for visualizing the dendritic tree. Synaptic puncta were brighter and could be distinguished from the dendrites. In contrast, in control mice injected with MSCV-Syn-GFP, labeled adult-born neurons showed more uniform expression along the dendrites, without punctate structures, further confirming that the synaptic punctate expression pattern is due to PSD95.FingR- and Gephyrin.FingR-directed binding to synaptic proteins. As expected, the PSD95.FingR expression was concentrated in the dendritic spines where over 90% of excitatory synapses are formed (Harris and Kater, 1994), whereas the Gephyrin.FingR puncta were generally confined to the dendritic shaft as described previously for inhibitory synapses (Chen et al., 2012; Kwon et al., 2018).

By examining MSCV-Syn-PSD95.FingR-GFP- and MSCV-Syn-Gephyrin.FingR-GFP-labeled neurons at different time points after viral injection, we were able to track excitatory and inhibitory synapse formation throughout the maturation period by euthanizing mice at 2, 4, and 12 weeks following cell birth (Figure 3C) (Toni and Sultan, 2011; van Praag et al., 2002). In PSD95.FingR-injected mice, we observed that although 2-week-old adult-born cells have developed dendrites protruding into the molecular layer, they have formed few excitatory synaptic puncta (12 $\pm$ 9 synapses per 100 μm, mean $\pm$ standard error, 4,709 μm dendrite length examined in 31 FOVs from 3 mice, Figures 3D and 3J). By 4 weeks of age, a significantly denser labeling was evident and mainly restricted to the dendritic spines, with a synaptic density of 97 $\pm$ 11 synapses per 100 μm (7,379 μm dendrite length, examined in 39 FOVs from 4 mice, Figures 3E and 3J, one-way ANOVA with post-hoc Bonferroni correction comparing 4 weeks versus 2 weeks, $p < 0.005$), consistent with previous studies (Sultan et al., 2015; Toni et al., 2007; van Praag et al., 2002). By 12 weeks of age, synapse density was further increased, but not significantly different from that at 4 weeks of age (132 $\pm$ 11 synapses per 100 μm, 7,657 μm dendrite length, examined in 35 FOVs from 3 mice at 12 weeks, Figures 3F and 3J, one-way ANOVA with post-hoc Bonferroni correction compared with that of 4 weeks, $p = 0.27$, compared with 2 weeks, $p < 0.001$).

Although dendritic spines outlined by soluble GFP expression have previously been used as a surrogate for excitatory synapses, it has not been possible to visualize inhibitory synapses based on morphology (Chen et al., 2012; Kwon et al., 2018). In mice injected with MSCV-Syn-Gephyrin.FingR-GFP, we found that 2-week-old adult-born neurons formed sparse GABAergic synaptic puncta along their dendrites (5 $\pm$ 3 synapses per 100 μm, 3,440 μm dendrite length examined in 27 FOVs from 3 mice, Figures 3G and 3K). By 4 weeks of age, we observed a moderate increase in the density of inhibitory synapses (13 $\pm$ 2 synapses per 100 μm, 14,341 μm dendrite length, examined in 50 FOVs from 4 mice, Figures 3H and 3K, one-way ANOVA with post-hoc Bonferroni correction comparing 4 weeks versus 2 weeks, $p = 0.066$), and at 12 weeks of age, the inhibitory synaptic density further increased to 16 $\pm$ 1 inhibitory synapses per 100 μm (4,635 μm

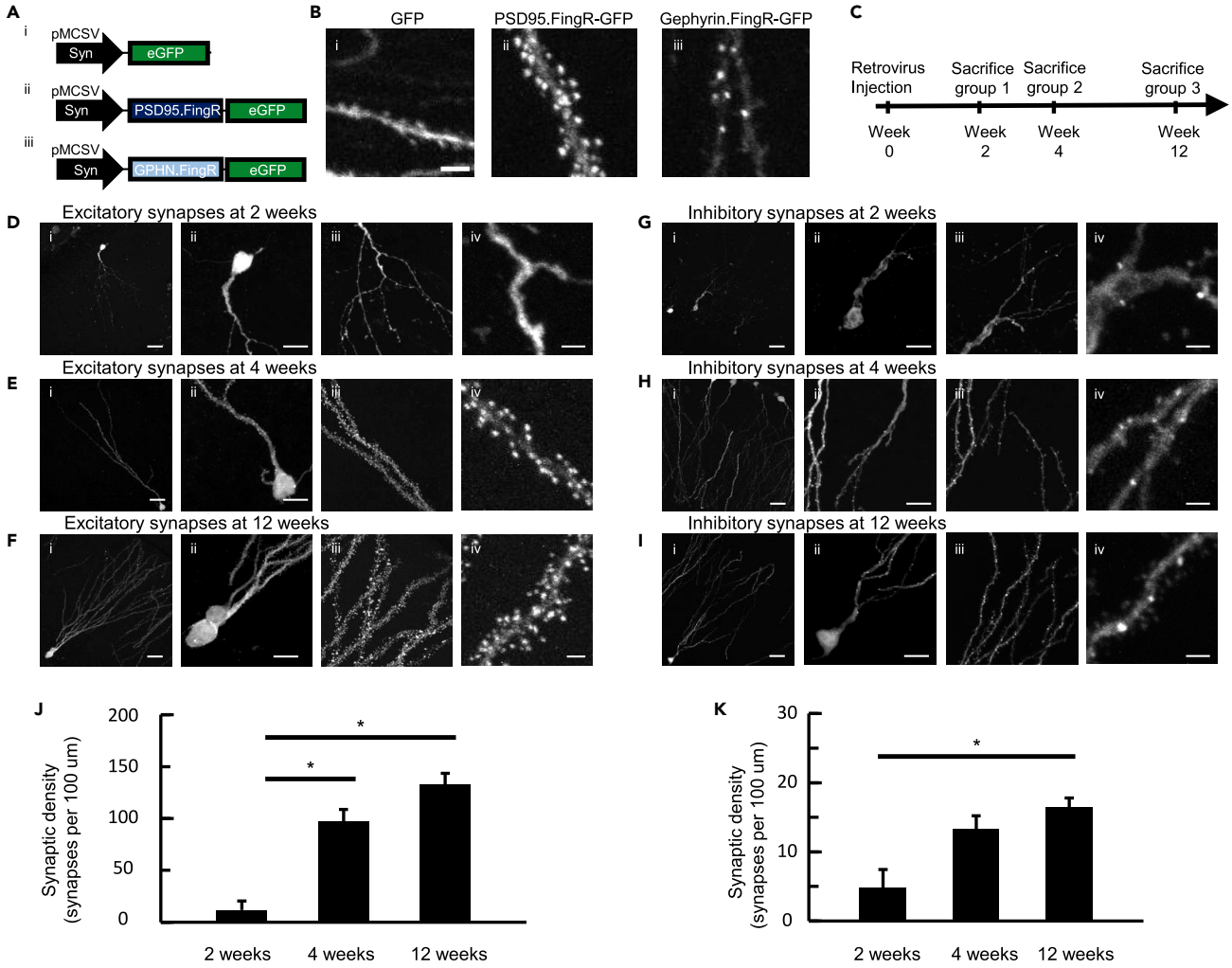

Figure 3. Retroviral FingRs Enable Tracking of Synaptic Development of Adult-Born Dentate Granule Cells throughout Maturation

(A) DNA construct diagrams for the retroviruses used in this study. (i) GFP control, (ii) PSD95.FingR-GFP (no transcriptional control), and (iii) Gephyrin.FingR-GFP (no transcriptional control).

(B) Representative images of (i) GFP, (ii) PSD95.FingR-GFP, and (iii) Gephyrin.FingR-GFP expression in 4-week-old adult-born cells. Scale bar, 2 μm.

(C) Timeline of retroviral injections and subsequent perfusion of mice for tracking synaptic development in adult-born neurons.

(D–F) Representative images of the expression patterns of PSD95.FingR-GFP in adult-born cells at 2 weeks (D), 4 weeks (E), and 12 weeks (F) following birth. Cells were imaged at 60× (i), 60× with a 4× zoom (ii and iii), and 60× with a 20× zoom (iv). Scale bars: 25 μm in (i), 10 μm in (ii and iii), and 2μm in (iv).

(G–I) Representative images of the expression patterns of Gephyrin.FingR-GFP in adult-born neurons at 2 weeks (G), 4 weeks (H), and 12 weeks (I) following birth. Cells were imaged at 60× (i), 60× with a 4× zoom (ii and iii), and 60× with a 20× zoom (iv). Scale bars: 25 μm in (i), 10 μm in (ii and iii), and 2 μm in (iv).

(J and K) Quantification of synaptic density (synapses per 100 μm) of excitatory (J) and inhibitory (K) synapses at 2, 4, and 12 weeks following cell birth (one-way ANOVA with post-hoc Bonferroni correction, *$p < 0.05$). Data represented as mean ± standard error.

dendrite length, examined in 27 FOVs from 3 mice, Figures 3I and 3K, one-way ANOVA with post-hoc Bonferroni correction compared to that of 4 weeks, $p = 0.69$, compared to 2 weeks, $p < 0.05$). Thus, for the development of both excitatory and inhibitory synapses, the largest increase in synaptic density occurred between weeks 2 and 4 with a more gradual increase between 4 and 12 weeks.

Cre-Inducible AAV FingR Viral Vectors Allow Synaptic Labeling of Striatal Aspiny Cholinergic Interneurons

Although several studies have explored the density of excitatory synaptic spines on projection neurons in the cortex, hippocampus, and striatum, little is known about the synaptic density of aspiny neurons, such as striatal cholinergic interneurons, due to the lack of spines. Striatal cholinergic interneurons only make up

1%–2% of striatal cells, but they have been implicated in movement behavior and learning (Gritton et al., 2019; Lim et al., 2014). To label the synapses of aspiny cholinergic interneurons, we generated cre-inducible AAV FingR vectors containing a double inverted operator (DIO). We co-injected AAV-DIO-mRuby2 and AAV-DIO-Gephyrin.FingR-GFP-CCR5TC to label inhibitory synapses, or AAV-DIO-mRuby2 and AAV-DIO-PSD95.FingR-GFP-CCR5TC to label excitatory synapses, into the striatum of ChAT-cre mice (Figures 4A and 4C). We found that AAV-DIO-mRuby2 labeled cholinergic interneurons' cell bodies and their dendrites uniformly red and AAV-DIO-Gephyrin.FingR-GFP-CCR5TC successfully labeled inhibitory synapses that appear in a punctate manner in green (Figure 4B). Similarly, AAV-DIO-PSD95.FingR-GFP-CCR5TC labeled excitatory synapses as green puncta (Figure 4D). We confirmed that mRuby2/FingR expression was limited to cholinergic interneurons using antibody staining as expected (Figure S7). The cre-lox system is a powerful tool for genetic targeting of distinct cell types expressing cre recombinase, and hundreds of transgenic cre mouse lines have been developed (Schnütgen et al., 2003). The AAV-DIO-FingRs generated here can be used with the vast number of cre-transgenic mouse lines to understand the synaptome of various cell types.

In dopamine-depleted Parkinson disease (PD) mouse models, it has been noted that the striatum undergoes synaptic reorganization in response to loss of dopaminergic input. Dopamine depletion leads to spine loss in inhibitory medium spiny neurons (MSNs) (Villalba et al., 2015), which could decrease MSN output to cholinergic neurons. We thus examined the impact of dopamine depletion on inhibitory synapses in cholinergic neurons. We co-injected cre-inducible AAV-DIO-mRuby2 and AAV-DIO-Gephyrin.FingR-GFP-CCR5TC into both hemispheres of the striatum in ChAT-cre mice. After 1 week, we unilaterally injected the neurotoxin 6-OHDA into the striatum to selectively deplete dopaminergic inputs to that hemisphere of striatum. Three weeks following the 6-OHDA injection, we validated dopamine depletion with tyrosine hydroxylase antibody staining (Figures 4E, 4F, and 4G, see Figure S7 for whole brain slice), and quantified the synaptic density in the lesioned versus non-lesioned hemispheres. Interestingly, we did not observe a noticeable difference in inhibitory synaptic density between the two hemispheres, suggesting that dopamine depletion does not result in inhibitory synaptic remodeling in striatal cholinergic interneurons 3 weeks after dopamine depletion (Figures 4F–4H). Together, these experiments demonstrate the breadth of studies enabled by these cre-inducible AAV FingR viral vectors in analyzing synaptic reorganization that accompanies disease models.

DISCUSSION

We engineered a viral toolbox of genetically encoded fluorescent synaptic tags that allow broad applications of FingR-based synaptic tagging of excitatory and inhibitory synapses in the mouse brain in a global or cell-specific manner. We screened a number of red-shifted reporter FingRs with RFPs fused to the N versus C terminus of the FingR and identified that N-terminally fused FingRs retained synaptic targeting specificity better than the C-terminally fused FingRs. The red FingR AAV viral vectors, when used in conjunction with the GFP-tagged green FingRs, allowed for dual-color synaptic labeling globally and can be applied in a cell-type-specific manner in cre-dependent transgenic mice. Furthermore, we explored the impact of transcriptional control in retroviral vector designs and found that the inclusion of transcriptional control elements diminished FingR expression in retroviral vectors due to the generally lower titer of the retrovirus compared with AAV viral vectors. By removing the transcriptional control, we generated FingR retroviral vectors that allowed us to estimate the density of excitatory and inhibitory synapses in adult-born granule cells during synaptic maturation. In addition, the cre-dependent AAV FingR variants enabled us to quantify the density of inhibitory synapses in cholinergic interneurons in healthy and diseased brains. Overall, the toolbox of FingR viral vectors generated here provides a powerful method for mapping the synaptome and understanding synaptic changes during development or plasticity related to learning or disease.

The development of the red Gephyrin.FingR demonstrates the possibility of engineering high-performance FingRs with different fluorophores. Our efforts highlight that not all fluorophores perform well when fused to FingRs, and certain variants, such as mCherry, interfere with FingRs binding to their protein target. In addition, we found that fluorophores fused to the N terminus of FingRs retained better synaptic targeting specificity than those fused to the C terminus. These results highlight the nuanced nature of molecular engineering, where a few mutations within the linker region between two protein domains could alter the functionality of the linked domains. For example, mutations at the linker region between GFP and the CaM-binding domain drastically altered the performance of the engineered genetically encoded calcium sensor GCaMP (Chen et al., 2013).

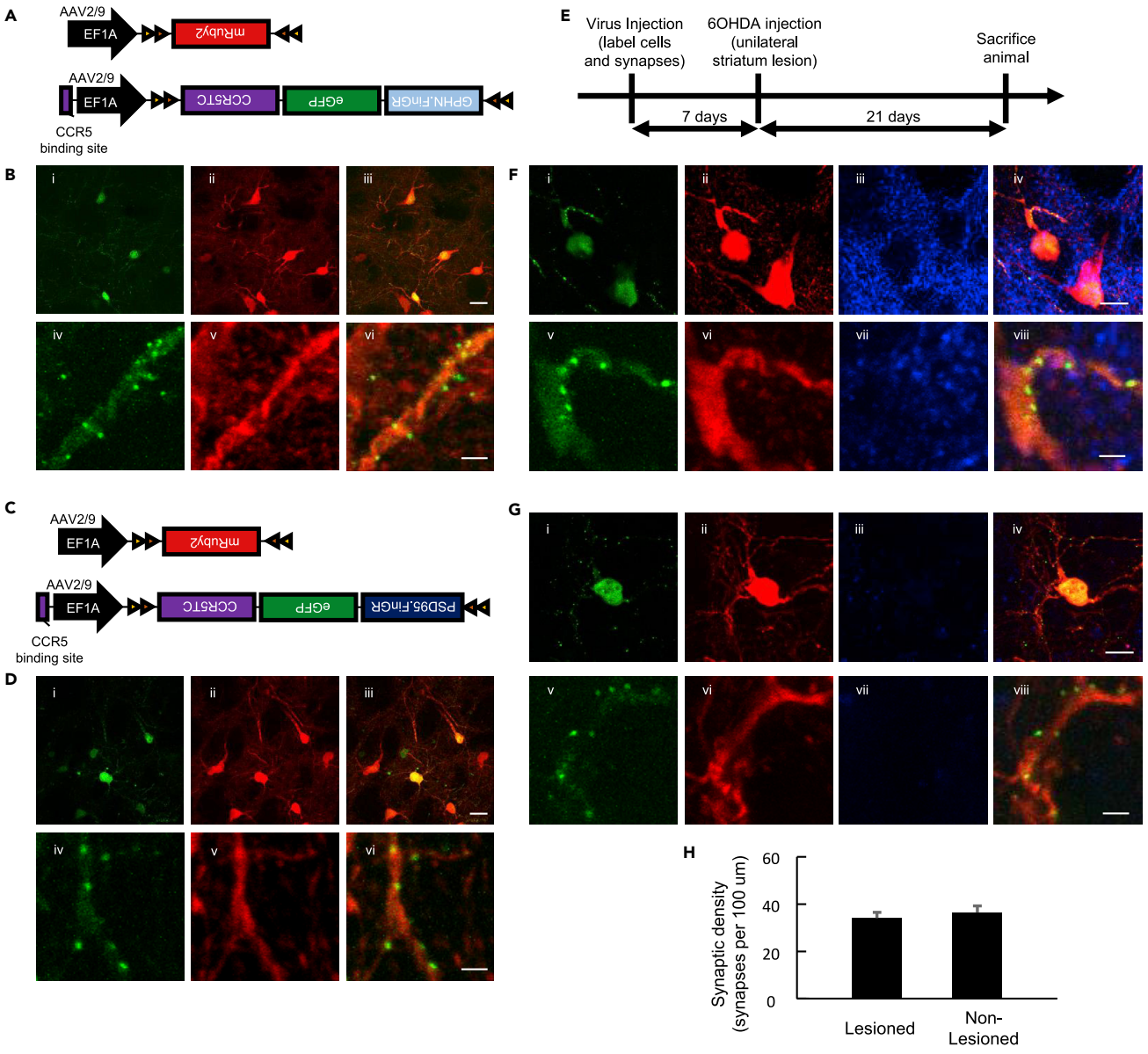

Figure 4. Cre-Inducible FingR Variants Label Synapses in Aspiny Striatal Cholinergic Interneurons

(A) DNA construct diagrams for labeling of cre-expressing neurons and their inhibitory synapses.

(B) 60× (i–iii) and 60× with 20× zoom (iv–vi) representative images of cholinergic interneurons with inhibitory synapses labeled in green (i and iv), cell bodies and dendrites labeled in red (ii and v), and a merge of both channels (iii and vi). Scale bars: 25 μm in (i–iii) and 2 μm in (iv–vi).

(C) DNA construct diagrams for labeling of neurons and excitatory synapses.

(D) 60× (i–iii) and 60× with 20× zoom (iv–vi) representative images of cholinergic interneurons with excitatory synapses labeled in green (i and iv), cell bodies and dendrites labeled in red (ii and v), and a merge of both channels (iii and vi). Scale bars: 25 μm in (i–iii) and 2 μm (iv–vi).

(E) Experimental timeline of virus injection, 6-OHDA injection, and perfusion of animals.

(F) Representative 60× with 4× zoom (top, i–iv) and 20× zoom (bottom, v–viii) images of a cholinergic interneuron with inhibitory synapses labeled with Gephyrin.FingR-GFP (i, v) and the whole cell labeled with mRuby2 (ii, vi) along with tyrosine hydroxylase (TH) staining for dopaminergic terminals (iii, vii); the overlay of the three images (iv, viii) in the non-lesioned hemisphere of striatum. Scale bar: 10 μm for images on the top and 2 μm for images on the bottom.

(G) Representative 60× with 4× zoom (top, i–iv) and 20× zoom (bottom, v–viii) images of a cholinergic interneuron with inhibitory synapses labeled with Gephyrin.FingR-GFP (i, v) and the whole cell labeled with mRuby2 (ii, vi) along with TH staining for dopaminergic terminals (iii, vii), the overlay of the three images (iv, viii) in the lesioned hemisphere of striatum. Scale bar, 10 μm for images on the top (i–iv) and 2μm for images on the bottom (v–viii).

(H) Quantification of inhibitory synaptic density in cholinergic interneurons with and without 6-OHDA lesioning. $p > 0.05$, no significant difference, Wilcoxon rank-sum test.

Data represented as mean ± standard error. For additional data, see also Figure S7.

Dual labeling of excitatory and inhibitory synapses is useful in understanding the excitation/inhibition balance in different brain regions and how this balance is altered during neuronal maturation or in disease states. The AAV FingRs can be stereotaxically delivered via intracranial injection to any brain region and can be confined to small structures by adjusting the volume of virus injected. Less-invasive synaptic labeling can also be performed by tail vein or facial vein injections of AAVs (Cearley and Wolfe, 2006; Foust et al., 2009; Zincarelli et al., 2008). In addition, AAV FingR labeling can help overcome the technical difficulty associated with the antibodies that cannot efficiently penetrate the densely packed post-synaptic density (Ryan and Grant, 2009; Sheng and Hoogenraad, 2007; Watanabe et al., 1998).

We found that similar to Gross et al. and Son et al., AAV viral vectors with transcriptional regulation of FingR protein expression yielded punctate expression in the dendrites and reduced background signal in the dendrites (Gross et al., 2013; Son et al., 2016). As expected, we also saw fluorescence in the cell nucleus due to the targeting of the FingR protein back to the nucleus for autoregulation. In addition, the PSD95.FingR and Gephyrin.FingR co-expressed in a punctate manner during dual synaptic labeling experiments, demonstrating that the two orthogonal zinc finger transcriptional control systems exhibited no cross talk when used in conjunction in the mouse brain. However, we found that the FingR retroviruses containing transcriptional control resulted in nearly no expression when tested, due to the generally lower titer of the retrovirus. By removing transcriptional control, the FingR retroviruses successfully tagged excitatory and inhibitory synapses. The low-level background fluorescent signal in the dendrites of retrovirus-labeled neurons in fact made it possible to visualize the individual cell from which each synapse was affiliated.

Although several studies have outlined the timeline of synaptic formation in adult neurogenesis, we here provide visualization of the location of inhibitory synapses and quantification of the density of inhibitory synapses during the maturation of these cells. Previously, inhibitory synapses were identified using electrophysiology and GABA agonists or antagonists (Esposito, 2005). Our data provide direct experimental evidence that the earliest GABAergic synapses form within 14 days after cell birth, and the number of synapses increases during maturation. Although GABA afferents are present as early as 1 week after birth, some cells do not develop functional synapses until after 2 weeks of age (Esposito, 2005). Electrophysiology studies suggest that perisomatic inhibitory synapses form in cells by 4 weeks after birth (Esposito, 2005; Toni and Sultan, 2011). Unfortunately, we were not able to accurately confirm this due to the higher concentration of Gephyrin.FingR protein in the soma. In addition, it is interesting that we found that the largest increase in inhibitory synaptic density comes between 2 and 4 weeks after cell birth, which coincides with the large increase in the number of excitatory synapses and the widely observed critical period. This could likely be a homeostatic mechanism for the cell to maintain its excitation/inhibition balance.

Many studies have explored the density of excitatory and inhibitory synapses in pyramidal cells in the cortex (Chen et al., 2012; Kwon et al., 2018; Villa et al., 2016) and tracked the absolute number and ratio of synapses in hippocampal pyramidal cells and interneurons (Gulyá et al., 1999; Megıas et al., 2001). In the striatum, most studies have focused on studying the number of spines on the MSNs (Day et al., 2006). Striatal cholinergic interneurons receive excitatory inputs from the cortex and thalamus, inhibitory inputs generally from the local MSNs and parvalbumin neurons, and dopaminergic inputs from the substantia nigra pars compacta (Ding et al., 2010; Lim et al., 2014). Recent studies have also identified inputs to cholinergic interneurons using monosynaptic tracing (Klug et al., 2018). Only two studies have specifically identified synapse density in striatal cholinergic interneurons, and this was done using electron microscopy (Sizemore et al., 2016, 2010). The ~0.36 inhibitory synapses per micron we found is consistent with the results reported in these two studies, but we were able to do this using confocal microscopy over broad regions of tissue, quantifying thousands of synapses with the FingRs, whereas the electron microscopy studies only examined tens of synapses (Sizemore et al., 2016, 2010).

We found no significant changes in the density of inhibitory synapses following 6-OHDA lesioning at 3 weeks, suggesting that dopamine depletion does not immediately induce plasticity changes at inhibitory synapses in cholinergic interneurons. However, because we only quantified synapses at one time point after dopamine depletion, it is unclear whether there is a simultaneous addition and subtraction of synapses that may be occurring or if depletion could result in a reduction in synapses over a longer timescale not analyzed here. Future studies using FingRs in different striatal cell types could provide a more comprehensive analysis of structural remodeling upon dopamine depletion.

One key advantage of the set of FingR viral vectors developed here are their flexibility for future studies. These viruses can be used in transgenic mice or combined with other viral vectors. In particular, the red FingR variants can be used to identify synapses while working with commonly used green fluorescent sensors such as GCaMP (Chen et al., 2013). The mScarlet and mRuby2 FingR tags developed here can be used in conjunction with near-infrared fluorescent proteins without spectral overlap (Filonov et al., 2011), allowing potential applications beyond dual color toward more color combinations. In addition, the development of a similar genetically encoded presynaptic tag will enable the study of synapses in greater detail. These probes are also compatible with super-resolution imaging methods such as PALM and STORM to further improve spatial resolution (Sinnen et al., 2017). Future studies with longitudinal *in vivo* imaging of the FingRs will yield insight into the formation and pruning of individual synapses over days and weeks. Finally, the FingRs can act as a targeting sequence for other genetically encoded tools to localize their expression to the synapses (Gross et al., 2016; Sinnen et al., 2017). We believe this toolbox of FingR viruses will prove useful for a variety of applications and enable numerous future neuroscience studies.

Limitations of the Study

In this study, the FingR viral vectors were tested in three major brain regions: the cortex, hippocampus, and striatum. We validated synaptic targeting using antibody co-localization in the hippocampus, but did not repeat this in all brain regions studied. However, the punctate expression patterns and higher density of PSD95.FingR-labeled synapses than Gephyrin.FingR-labeled synapse suggest that the FingR vectors correctly identify excitatory and inhibitory synapses. Furthermore, the synaptic densities we report for excitatory synapses in adult-born granule cells and for inhibitory synapses in striatal cholinergic interneurons are in line with previous studies (Sizemore et al., 2016, 2010; Sultan et al., 2015; Toni et al., 2007; van Praag et al., 2002).

Although we demonstrated that dual-color labeling of excitatory and inhibitory synapses in the same neurons is possible as shown in Figure 2, this current study did not include red variants of the retroviral or AAV cre-inducible FingR vectors. In addition, whereas we examined inhibitory synapse formation on dendrites in adult-born granule cells (Figure 3), we were not able to look at synapses on the soma of adult-born granule cells due to the buildup of fluorescent protein in the cell body without transcriptional control. As noted in the earlier discussion, the addition of a transcriptional control unit greatly diminished the overall fluorescence of the FingR proteins in retroviral vectors, making it difficult to identify individual synapses in adult-born granule cells.

We quantified synaptic densities in adult-born granule cells and dopamine-depleted aspiny striatal cholinergic interneurons over time in fixed brain sections, and thus we were able to capture the synaptic density only at a given time point in each animal. However, this is a limitation of the quantification techniques used in this study, rather than the FingR viral vectors. Deploying high-resolution *in vivo* imaging techniques, future studies should be able to track dynamic changes of synapses over time in the same animal.

Resource Availability

Lead Contact

Additional resources related to this study are available upon reasonable request from the Lead Contact (Xue Han, xuehan@bu.edu).

Materials Availability

Plasmids used in this study and their sequences are available at Addgene.org (AAV-EF1A-PSD95.FingR-eGFP-CCR5TC, 125691; AAV-EF1A-Gephyrin.FingR-eGFP-CCR5TC, 125692; AAV-Syn-PSD95.FingR-eGFP-CCR5TC, 125693; AAV-Syn-PSD95-mCherry, 125694; AAV-EF1A-mScarlet-Gephyrin.FingR-IL2RGTC, 125695; AAV- EF1A-mRuby2-Gephyrin.FingR-IL2RGTC, 125696; MSCV-Syn-PSD95.FingR-eGFP, 126212; MSCV-Syn-Gephyrin.FingR-eGFP, 126213; AAV-EF1A-DIO-mRuby2, 126215; AAV-EF1A-DIO-PSD95.FingR-eGFP-CCR5TC, 126216; AAV-EF1A-DIO-Gephyrin.FingR-eGFP-CCR5TC, 126217; Lenti-CamKII-PSD95.FingR-eGFP-CCR5TC, 126218).

Data and Code Availability

The data used in this study are available upon reasonable request from the Lead Contact (Xue Han, xuehan@bu.edu). Computer code used to generate results for this study is available at https://github.com/HanLabBU/Synaptic-puncta-quantification. Sequences of the generated DNA plasmids are available

at GenBank via the following accession numbers: GenBank: MT586119 for AAV-EF1A-mScarlet-Gephyrin.FingR-IL2RGTC; GenBank: MT612428 for AAV-EF1A-mRuby2-Gephyrin.FingR-IL2RGTC; MT612429 for AAV-EF1A-PSD95.FingR-GFP-CCR5TC; GenBank: MT612430 for AAV-EF1A-DIO-PSD95.FingR-GFP-CCR5TC; GenBank: MT612431 for AAV-EF1A-DIO-Gephyrin.FingR-GFP-CCR5TC; GenBank: MT612432 for AAV-EF1A-Gephyrin.FingR-GFP-CCR5TC; GenBank: MT612433 for MSCV-syn-PSD95.FingR-GFP; and GenBank: MT612434 for MSCV-syn-Gephyrin.FingR-GFP.

METHODS

All methods can be found in the accompanying Transparent Methods supplemental file.

SUPPLEMENTAL INFORMATION

Supplemental Information can be found online at https://doi.org/10.1016/j.isci.2020.101330.

ACKNOWLEDGMENTS

We thank J.P. Gilbert, Yuda Huo, and Margaret O'Connor for providing neuron cultures. We also thank the Boston University Micro and Nano Imaging Facility for providing access to the confocal microscope (supported by NIH S10OD024993). X.H. acknowledges funding from the NIH Director's Office (1DP2NS082126), NINDS (1R01NS109794, R21MH109941, R01NS087950), and NSF CBET-1848029. S.B., S.N.S., and R.A.M. acknowledge funding from the NIH/NIGMS T32 Quantitative Biology and Physiology Fellowship (GM008764) through the Boston University Biomedical Engineering Department. S.N.S acknowledges NIH F31 NS115421. S.S., H.V., and C.B. acknowledge funding support from the Boston University UROP program.

AUTHOR CONTRIBUTIONS

S.B. and X.H. conceived of and designed all experiments and wrote the manuscript. X.H. supervised the study. S.B., S.S., H.V., S.N.S., R.A.M., and C.B. performed all molecular cloning. S.B., with help from H.V., packaged the viruses. S.B., T.L.T., and K.H.C. performed animal surgeries. H.J.G. provided transgenic animals and comments on experimental design. S.B., S.S., H.J.G., and T.L.T. performed immunohistology. S.B., S.S., and T.L.T. performed confocal imaging. S.B., S.S., with help from D.Z., P.F., and K.H.C., performed data analysis. H.-Y.M provided neuron cultures and comments on experimental design. All authors helped edit the manuscript.

DECLARATION OF INTERESTS

The authors declare no competing financial interests.

Received: April 21, 2019
Revised: April 18, 2020
Accepted: June 26, 2020
Published: July 24, 2020

REFERENCES

Bindels, D.S., Haarbosch, L., van Weeren, L., Postma, M., Wiese, K.E., Mastop, M., Aumonier, S., Gotthard, G., Royant, A., Hink, M.A., and Gadella, T.W.J., Jr. (2017). mScarlet: a bright monomeric red fluorescent protein for cellular imaging. Nat. Methods *14*, 1–12.

Bosch, M., Castro, J., Saneyoshi, T., Matsuno, H., Sur, M., and Hayashi, Y. (2014). Structural and molecular remodeling of dendritic spine substructures during long-term potentiation. Neuron *82*, 444–459.

Broadhead, M.J., Horrocks, M.H., Zhu, F., Muresan, L., Benavides-Piccione, R., DeFelipe, J., Fricker, D., Kopanitsa, M.V., Duncan, R.R., Klenerman, D., et al. (2016). PSD95 nanoclusters are postsynaptic building blocks in hippocampus circuits. Sci. Rep. *6*, 24626.

Cane, M., Maco, B., Knott, G., and Holtmaat, A. (2014). The relationship between PSD-95 clustering and spine stability in vivo. J. Neurosci. *34*, 2075–2086.

Cearley, C.N., and Wolfe, J.H. (2006). Transduction characteristics of adeno-associated virus vectors expressing cap serotypes 7, 8, 9, and Rh10 in the mouse brain. Mol. Ther. *13*, 528–537.

Chen, J.L., Villa, K.L., Cha, J.W., So, P.T.C., Kubota, Y., and Nedivi, E. (2012). Clustered dynamics of inhibitory synapses and dendritic spines in the adult neocortex. Neuron *74*, 361–373.

Chen, T.W., Wardill, T.J., Sun, Y., Pulver, S.R., Renninger, S.L., Baohan, A., Schreiter, E.R., Kerr, R.A., Orger, M.B., Jayaraman, V., et al. (2013). Ultrasensitive fluorescent proteins for imaging neuronal activity. Nature *499*, 295–300.

Chen, Y., Akin, O., Nern, A., Tsui, C.Y.K., Pecot, M.Y., and Zipursky, S.L. (2014). Cell-type-specific labeling of synapses in vivo through synaptic tagging with recombination. Neuron *81*, 280–293.

Dani, A., Huang, B., Bergan, J., Dulac, C., and Zhuang, X. (2010). Superresolution imaging of chemical synapses in the brain. Neuron *68*, 843–856.

Danielson, N.B.B., Kaifosh, P., Zaremba, J.D.D., Lovett-Barron, M., Tsai, J., Denny, C.A.A.,

Balough, E.M.M., Goldberg, A.R.R., Drew, L.J.J., Hen, R., et al. (2016). Distinct contribution of adult-born hippocampal granule cells to context encoding. Neuron *90*, 101–112.

Day, M., Wang, Z., Ding, J., An, X., Ingham, C.A., Shering, A.F., Wokosin, D., Ilijic, E., Sun, Z., Sampson, A.R., et al. (2006). Selective elimination of glutamatergic synapses on striatopallidal neurons in Parkinson disease models. Nat. Neurosci. *9*, 251–259.

Ding, J.B., Guzman, J.N., Peterson, J.D., Goldberg, J.A., and Surmeier, D.J. (2010). Thalamic gating of corticostriatal signaling by cholinergic interneurons. Neuron *67*, 294–307.

El-Husseini, A., Schnell, E., and Chetkovich, D. (2000). PSD-95 involvement in maturation of excitatory synapses. Science *290*, 1364–1368.

Esposito, M.S. (2005). Neuronal differentiation in the adult hippocampus recapitulates embryonic development. J. Neurosci. *25*, 10074–10086.

Filonov, G.S., Piatkevich, K.D., Ting, L., Zhang, J., Kim, K., and Verkhusha, V.V. (2011). Bright and stable near-infrared fluorescent protein for in vivo imaging. Nat. Biotechnol. *29*, 759–763.

Fortin, D.a., Tillo, S.E., Yang, G., Rah, J.-C.J.-C., Melander, J.B., Bai, S., Soler-Cedeno, O., Qin, M., Zemelman, B.V., Guo, C., et al. (2014). Live imaging of endogenous PSD-95 using ENABLED: a conditional strategy to fluorescently label endogenous proteins. J. Neurosci. *34*, 16698–16712.

Foust, K.D., Nurre, E., Montgomery, C.L., Hernandez, A., Chan, C.M., and Kaspar, B.K. (2009). Intravascular AAV9 preferentially targets neonatal neurons and adult astrocytes. Nat. Biotechnol. *27*, 59–65.

Fritschy, J.-M., Weinmann, O., Wenzel, A., and Benke, D. (1998). Synapse-specific localization of NMDA and GABA A receptor subunits revealed by antigen-retrieval. J. Comp. Neurol. *390*, 194–210.

Fukaya, M., and Watanabe, M. (2000). Improved immunohistochemical detection of postsynaptically located PSD-95/SAP90 protein family by protease section pretreatment: a study in the adult mouse brain. J. Comp. Neurol. *426*, 572–586.

Ge, S., Yang, C.H., Hsu, K.S., Ming, G.L., and Song, H. (2007). A critical period for enhanced synaptic plasticity in newly generated neurons of the adult brain. Neuron *54*, 559–566.

Gritton, H.J., Howe, W.M., Romano, M.F., DiFeliceantonio, A.G., Kramer, M.A., Saligrama, V., Bucklin, M.E., Zemel, D., and Han, X. (2019). Unique contributions of parvalbumin and cholinergic interneurons in organizing striatal networks during movement. Nat. Neurosci. *22*, 586–597.

Gross, G.G., Junge, J.a., Mora, R.J., Kwon, H.-B., Olson, C.A., Takahashi, T.T., Liman, E.R., Ellis-Davies, G.C.R., McGee, A.W., Sabatini, B.L., et al. (2013). Recombinant probes for visualizing endogenous synaptic proteins in living neurons. Neuron *78*, 971–985.

Gross, G.G., Straub, C., Perez-Sanchez, J., Dempsey, W.P., Junge, J.A., Roberts, R.W., Trinh, L.A., Fraser, S.E., De Koninck, Y., De Koninck, P., et al. (2016). An E3-ligase-based method for ablating inhibitory synapses. Nat. Methods *13*, 673–678.

Gulyá, A.I., Megías, M., Emri, Z., and Freund, T.F. (1999). Total number and ratio of excitatory and inhibitory synapses converging onto single interneurons of different types in the CA1 area of the rat hippocapus. J. Neurosci. *19*, 10082–10097.

Gutierrez-Mecinas, M., Kuehn, E.D., Abraira, V.E., Polgár, E., Watanabe, M., and Todd, A.J. (2016). Immunostaining for Homer reveals the majority of excitatory synapses in laminae I-III of the mouse spinal dorsal horn. Neuroscience *329*, 171–181.

Harris, K.M., and Kater, S.B. (1994). Dendritic spines: cellular specializations imparting both stability and flexibility to synaptic function. Annu. Rev. Neurosci. *17*, 341–371.

Kannan, M., Gross, G.G., Arnold, D.B., and Higley, M.J. (2016). Visual deprivation during the critical period enhances layer 2/3 GABAergic inhibition in mouse V1. J. Neurosci. *36*, 5914–5919.

Kim, J., Zhao, T., Petralia, R.S., Yu, Y., Peng, H., Myers, E., and Magee, J.C. (2011). mGRASP enables mapping mammalian synaptic connectivity with light microscopy. Nat. Methods *9*, 96–102.

Klug, J.R., Engelhardt, M.D., Cadman, C.N., Li, H., Smith, J.B., Ayala, S., Williams, E.W., Hoffman, H., and Jin, X. (2018). Differential inputs to striatal cholinergic and parvalbumin interneurons imply functional distinctions. Elife *7*, 1–25.

Kwon, T., Merchán-Pérez, A., Rial Verde, E.M., Rodríguez, J.-R., DeFelipe, J., and Yuste, R. (2018). Ultrastructural, molecular and functional mapping of GABAergic synapses on dendritic spines and shafts of neocortical pyramidal neurons. Cereb. Cortex *29*, 2771–2781.

Lam, A.J., St-Pierre, F., Gong, Y., Marshall, J.D., Cranfill, P.J., Baird, M.a., McKeown, M.R., Wiedenmann, J., Davidson, M.W., Schnitzer, M.J., et al. (2012). Improving FRET dynamic range with bright green and red fluorescent proteins. Nat. Methods *9*, 1005–1012.

Lichtman, J.W., Sanes, J.R., Cohen, K.B., Luo, T., and Cai, D. (2013). Improved tools for the Brainbow toolbox. Nat. Methods *10*, 540–547.

Lim, S.A.O., Kang, U.J., and McGehee, D.S. (2014). Striatal cholinergic interneuron regulation and circuit effects. Front. Synaptic Neurosci. *6*, 1–23.

Macpherson, L.J., Zaharieva, E.E., Kearney, P.J., Alpert, M.H., Lin, T.-Y., Turan, Z., Lee, C.-H., and Gallio, M. (2015). Dynamic labelling of neural connections in multiple colours by trans-synaptic fluorescence complementation. Nat. Commun. *6*, 10024.

Masch, J.-M., Steffens, H., Fischer, J., Engelhardt, J., Hubrich, J., Keller-Findeisen, J., D'Este, E., Urban, N.T., Grant, S.G.N., Sahl, S.J., et al. (2018). Robust nanoscopy of a synaptic protein in living mice by organic-fluorophore labeling. Proc. Natl. Acad. Sci. U S A *115*, E8047–E8056.

Megıas, M., Emri, Z., Freund, T., and Gulyás, A. (2001). Total number and distribution of inhibitory and excitatory synapses on hippocampal CA1 pyramidal cells. Neuroscience *102*, 527–540.

Meyer, D., Bonhoeffer, T., and Scheuss, V. (2014). Balance and stability of synaptic structures during synaptic plasticity. Neuron *82*, 430–443.

Nakashiba, T., Cushman, J.D., Pelkey, K.A., Renaudineau, S., Buhl, D.L., McHugh, T.J., Rodriguez Barrera, V., Chittajallu, R., Iwamoto, K.S., McBain, C.J., et al. (2012). Young dentate granule cells mediate pattern separation, whereas old granule cells facilitate pattern completion. Cell *149*, 188–201.

Ryan, T.J., and Grant, S.G.N. (2009). The origin and evolution of synapses. Nat. Rev. Neurosci. *10*, 701–712.

Schmidt-Hieber, C., Jones, P., and Bischofberger, J. (2004). Enhanced synaptic plasticity in newly generated granule cells of the adult hippocampus. Nature *429*, 184–187.

Schnütgen, F., Doerflinger, N., Calléja, C., Wendling, O., Chambon, P., and Ghyselinck, N.B. (2003). A directional strategy for monitoring Cre-mediated recombination at the cellular level in the mouse. Nat. Biotechnol. *21*, 562–565.

Shaner, N.C., Campbell, R.E., Steinbach, P.A., Giepmans, B.N.G., Palmer, A.E., and Tsien, R.Y. (2004). Improved monomeric red, orange and yellow fluorescent proteins derived from Discosoma sp. red fluorescent protein. Nat. Biotechnol. *22*, 1567–1572.

Sheng, M., and Hoogenraad, C.C. (2007). The postsynaptic architecture of excitatory synapses: a more quantitative view. Annu. Rev. Biochem. *76*, 823–847.

Sinnen, B.L., Bowen, A.B., Forte, J.S., Hiester, B.G., Crosby, K.C., Gibson, E.S., Dell'Acqua, M.L., and Kennedy, M.J. (2017). Optogenetic control of synaptic composition and function. Neuron *93*, 646–660.e5.

Sizemore, R.J., Reynolds, J.N.J., and Oorschot, D.E. (2010). Number and type of synapses on the distal dendrite of a rat striatal cholinergic interneuron: a quantitative, ultrastructural study. J. Anat. *217*, 223–235.

Sizemore, R.J., Zhang, R., Lin, N., Goddard, L., Wastney, T., Parr-Brownlie, L.C., Reynolds, J.N.J., and Oorschot, D.E. (2016). Marked differences in the number and type of synapses innervating the somata and primary dendrites of midbrain dopaminergic neurons, striatal cholinergic interneurons, and striatal spiny projection neurons in the rat. J. Comp. Neurol. *524*, 1062–1080.

Sjulson, L., Cassataro, D., DasGupta, S., and Miesenböck, G. (2016). Cell-specific targeting of genetically encoded tools for neuroscience. Annu. Rev. Genet. *50*, 571–594.

Son, J.-H., Keefe, M.D., Stevenson, T.J., Barrios, J.P., Anjewierden, S., Newton, J.B., Douglass, A.D., and Bonkowsky, J.L. (2016). Transgenic FingRs for live mapping of synaptic dynamics in genetically-defined neurons. Sci. Rep. *6*, 18734.

Specht, C.G., Izeddin, I., Rodriguez, P.C., ElBeheiry, M., Rostaing, P., Darzacq, X., Dahan, M., and Triller, A. (2013). Quantitative nanoscopy of inhibitory synapses: counting gephyrin

molecules and receptor binding sites. Neuron *79*, 308–321.

Sultan, S., Li, L., Moss, J., Petrelli, F., Cassé, F., Gebara, E., Lopatar, J., Pfrieger, F.W., Bezzi, P., Bischofberger, J., and Toni, N. (2015). Synaptic integration of adult-born hippocampal neurons is locally controlled by astrocytes. Neuron *88*, 957–972.

Tepper, J.M., Abercrombie, E.D., and Bolam, J.P. (2007). Basal ganglia macrocircuits. Prog. Brain Res. *160*, 3–7.

Toni, N., and Sultan, S. (2011). Synapse formation on adult-born hippocampal neurons. Eur. J. Neurosci. *33*, 1062–1068.

Toni, N., Teng, E.M., Bushong, E.A., Aimone, J.B., Zhao, C., Consiglio, A., van Praag, H., Martone, M.E., Ellisman, M.H., and Gage, F.H. (2007). Synapse formation on neurons born in the adult hippocampus. Nat. Neurosci. *10*, 727–734.

van Praag, H., Schinder, A.F., Christie, B.R., Toni, N., Palmer, T.D., and Gage, F.H. (2002). Functional neurogenesis in the adult hippocampus. Nature *415*, 1030–1034.

Villa, K.L., Berry, K.P., Subramanian, J., Cha, J.W., Oh, W.C., Kwon, H.B., Kubota, Y., So, P.T.C., and Nedivi, E. (2016). Inhibitory synapses are repeatedly assembled and removed at persistent sites in vivo. Neuron *89*, 756–769.

Villalba, R.M., Mathai, A., and Smith, Y. (2015). Morphological changes of glutamatergic synapses in animal models of Parkinson's disease. Front. Neuroanat. *9*, 117.

Walker, A.S., Neves, G., Grillo, F., Jackson, R.E., Rigby, M., O'Donnell, C., Lowe, A.S., Vizcay-Barrena, G., Fleck, R.A., and Burrone, J. (2017). Distance-dependent gradient in NMDAR-driven spine calcium signals along tapering dendrites. Proc. Natl. Acad. Sci. U S A *114*, E1986–E1995.

Watanabe, M., Fukaya, M., Sakimura, K., Manabe, T., Mishina, M., and Inoue, Y. (1998). Selective scarcity of NMDA receptor channel subunits in the stratum lucidum (mossy fibre-recipient layer) of the mouse hippocampal CA3 subfield. Eur. J. Neurosci. *10*, 478–487.

Zhao, C., Teng, E.M., Summers, R.G., Jr., Ming, G., and Gage, F.H. (2006). Distinct morphological stages of dentate granule neuron maturation in the adult mouse hippocampus. J. Neurosci. *26*, 3–11.

Zhu, F., Cizeron, M., Qiu, Z., Benavides-Piccione, R., Kopanitsa, M.V., Skene, N.G., Koniaris, B., DeFelipe, J., Fransén, E., Komiyama, N.H., and Grant, S.G.N. (2018). Architecture of the mouse brain synaptome. Neuron *99*, 781–799.e10.

Zhuo, J.M., Tseng, H.A., Desai, M., Bucklin, M.E., Mohammed, A.I., Robinson, N.T., Boyden, E.S., Rangel, L.M., Jasanoff, A.P., Gritton, H.J., and Han, X. (2016). Young adult born neurons enhance hippocampal dependent performance via influences on bilateral networks. Elife *5*, 25.

Zincarelli, C., Soltys, S., Rengo, G., and Rabinowitz, J.E. (2008). Analysis of AAV serotypes 1-9 mediated gene expression and tropism in mice after systemic injection. Mol. Ther. *16*, 1073–1080.

iScience, Volume *23*

Supplemental Information

A Viral Toolbox of Genetically Encoded Fluorescent Synaptic Tags

Seth Bensussen, Sneha Shankar, Kimberley H. Ching, Dana Zemel, Tina L. Ta, Rebecca A. Mount, Sanaya N. Shroff, Howard J. Gritton, Pierre Fabris, Hannah Vanbenschoten, Connor Beck, Heng-Ye Man, and Xue Han

Supplementary Information

Supplementary Table 1. Viral constructs generated in this study, related to Figures 1-4.

AAV-EF1A-PSD95.FingR-eGFP-CCR5TC
AAV-EF1A-Gephyrin.FingR-eGFP-CCR5TC
AAV-Syn-PSD95.FingR-eGFP-CCR5TC
AAV-Syn-PSD95-mCherry
AAV-EF1A-Gephyrin.FingR-mScarlet-IL2RGTC
AAV-EF1A-mScarlet-Gephyrin.FingR- IL2RGTC
AAV-EF1A-mRuby2-Gephyrin.FingR- IL2RGTC
AAV-EF1A-mCherry-Gephyrin.FingR- IL2RGTC
MSCV-Syn-eGFP
MSCV-Syn-PSD95.FingR-GFP
MSCV-Syn-Gephyrin.FingR-GFP
AAV-EF1A-DIO-mRuby2
AAV-EF1A-DIO-PSD95.FingR-eGFP-CCR5TC
AAV-EF1A-DIO-Gephyrin.FingR-eGFP-IL2RGTC
Lenti-CamKII-PSD95.FingR-eGFP-CCR5TC
Lenti-CamKII-Gephyrin.FingR-mRuby2-IL2RGTC
MSCV-Syn-PSD95.FingR-eGFP-CCR5TC
MSCV-Syn-Gephyrin.FingR-mRuby2-IL2RGTC

Supplementary Figure 1. Validation of PSD95.FingR AAV labeling of excitatory synapses, related to Figure 1.

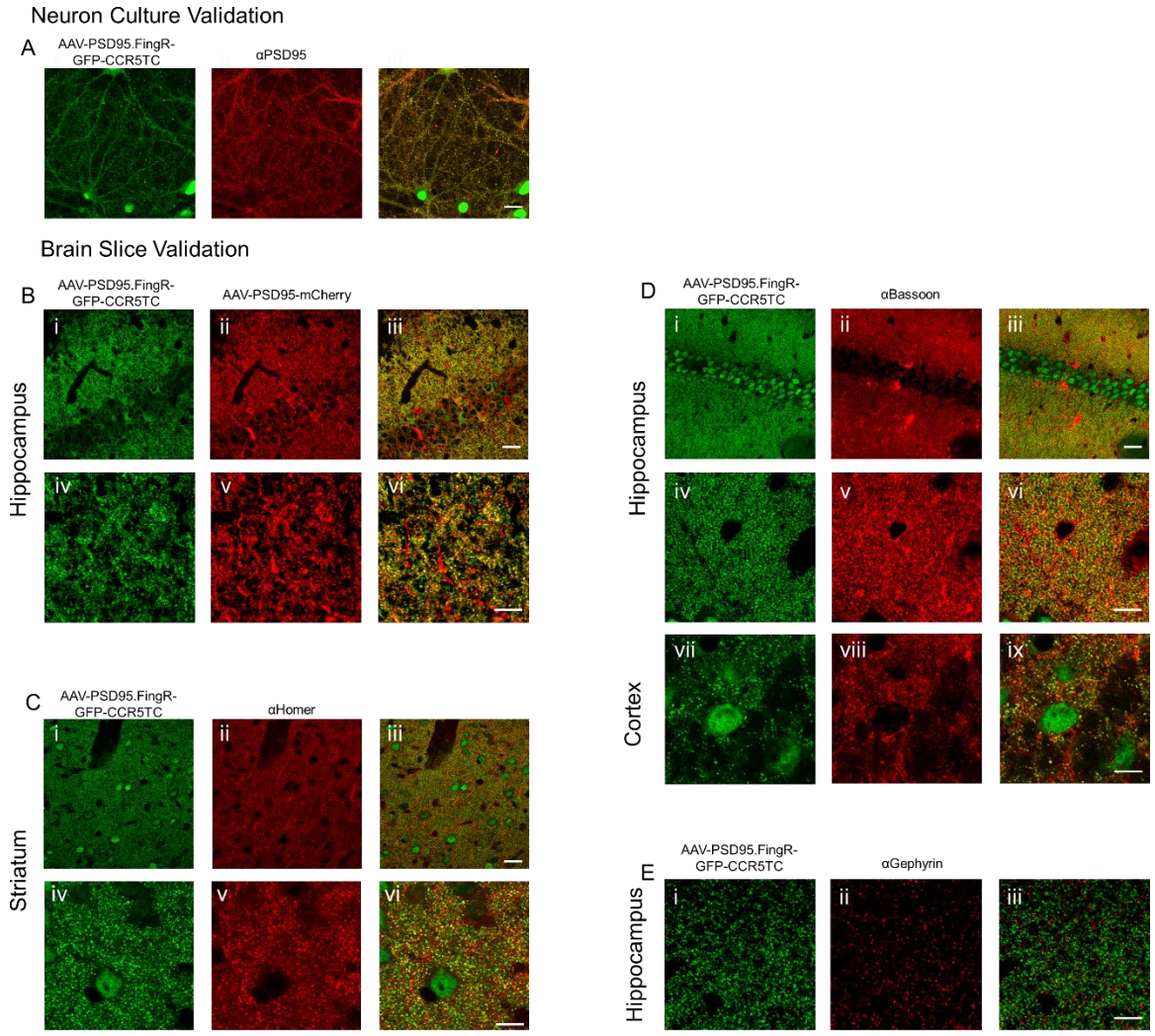

A) PSD95.FingR-GFP co-localizes with the PSD95 antibody in neuron culture. Scale bar 25um. (B-E) PSD95.FingR-GFP expression patterns in mouse brain slices. B) PSD95.FingR-GFP co-localizes with exogenously expressed PSD95-mCherry. Representative images at 60x (i-iii) and 60x with 4x zoom (iv-vi). Scale bars 25um (i-iii) and 10um (iv-vi). C) PSD95.FingR-GFP co-localizes with the antibody Homer, a marker of metabotropic glutamate receptors. Representative images at 60x (i-iii) and 60x with 4x zoom (iv-vi). Scale bar 25um (i-iii) and 10um (iv-vi). D) PSD95.FingR-GFP co-localizes with the antibody bassoon, a marker of pre-synaptic terminals. Representative images in the hippocampus at 60x (i-iii) and 60x with 4x zoom (iv-vi) and in the cortex at 60x with 4x zoom (vii-ix). Scale bars 25um (i-iii) and 10um (iv-ix). E) PSD95.FingR-GFP does not co-localize with the antibody gephyrin, a marker of inhibitory synapses. Scale bar 10um.

Supplementary Figure 2. Expression patterns of AAV PSD95.FingR-GFP under the synapsin promoter in multiple brain regions, related to Figure 1.

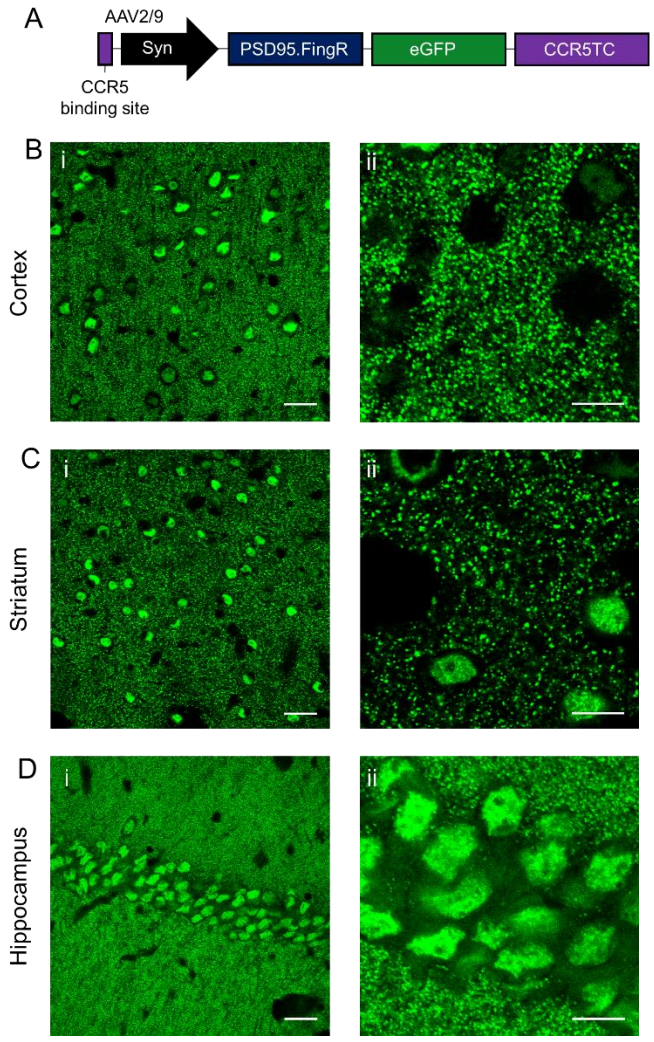

A) Viral DNA construct diagram. PSD95.FingR-GFP expression under the neuron specific synapsin promoter exhibit punctate expression patterns in cortex (B), striatum (C), and hippocampus (D). FingR AAVs were injected into the mouse brain and analyzed 3 weeks following injection. Representative images at 60x (i) and 60x with 4x zoom (ii). Scale bars 25um (i) and 10um (ii).

Supplementary Figure 3. Expression of lentivirus mediated PSD95.FingR-GFP and Gephyrin.FingR-mRuby2, related to Figure 1.

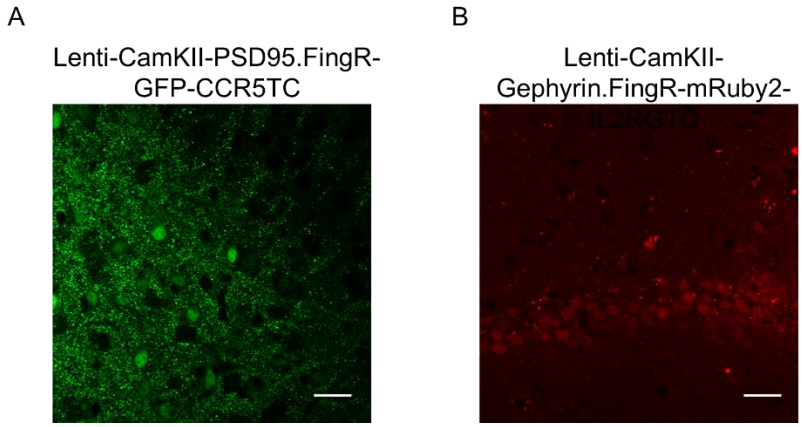

FingR lentiviruses were injected into the mouse brain and analyzed 2 weeks following injection. The PSD95.FingR-GFP lentivirus labeled cell nuclei and expressed in a punctate manner in the dendrites (A), but the overall expression was weak. The Gephyrin.FingR-mRuby2 lentivirus faintly labeled cell nuclei but did not appear to label inhibitory synapses in the cell dendrites (B). Scale bars 25um.

Supplementary Figure 4. Dual color labeling of excitatory and inhibitory synapses with PSD95.FingR-GFP and the four red Gephyrin.FingR variants, related to Figure 2.

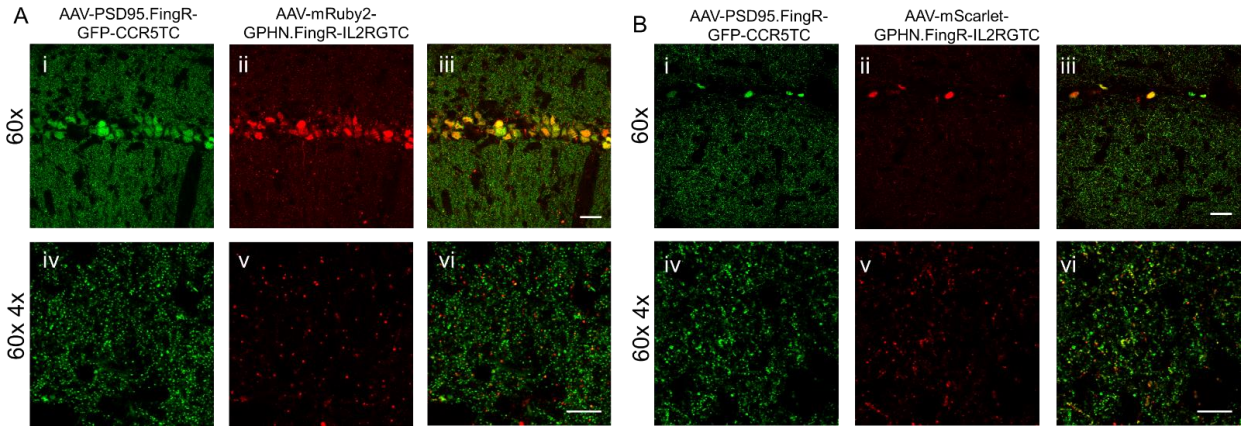

AAV-PSD95.FingR-GFP-CCR5TC was co-injected into the hippocampus with A) AAV-mRuby2-Gephyrin.FingR-IL2RGTC, and B) AAV-mScarlet-Gephyrin.FingR-IL2RGTC. GFP expression pattern was shown in (i), red fluorescent protein expression was shown in (ii) and merge (iii). Scale bars are 25µm (i-iii) and 10µm (iv-vi).

Supplementary Figure 5. Antibody staining of dual synaptic labeling, related to Figure 2.

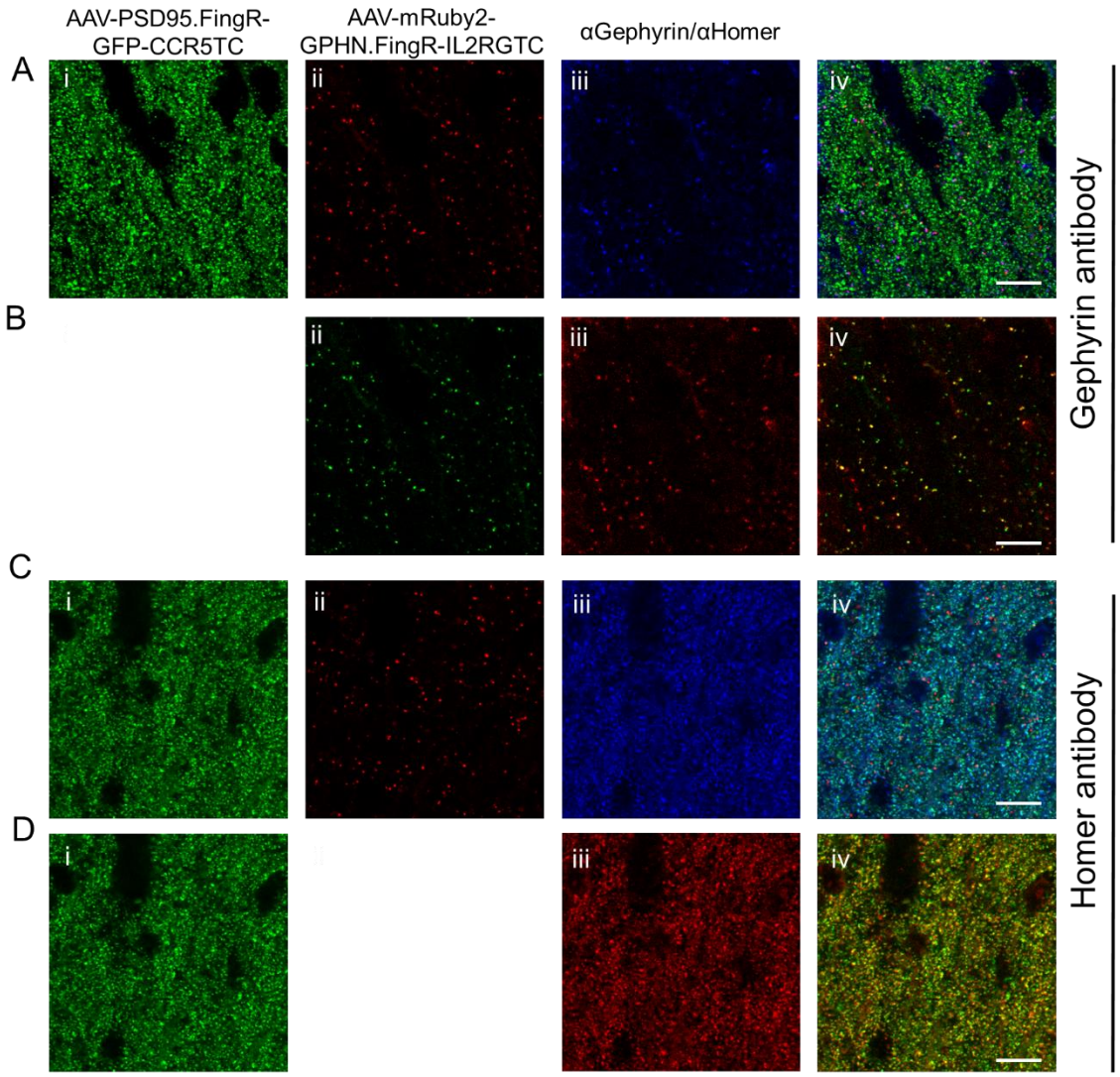

Brain slices co-injected with AAV-PSD95.FingR-GFP-CCR5TC (i) and AAV-mRuby2-Gephyrin.FingR-IL2RGTC (ii) were stained with gephyrin (A, B (iii)) or homer (C, D (iii)) antibodies to validate the corresponding synaptic labeling patterns (iv). B) The Gephyrin.FingR was pseudocolored green (ii) and the gephyrin antibody fluorescence was pseudocolored red (iii), and the merge was shown to visualize co-localization (iv). D) The PSD95.FingR expression was pseudocolored green (ii) and the homer antibody fluorescence was pseudocolored red (iii), and the merge was shown to visualize co-localization (iv). Scale bars 10um.

Supplementary Figure 6. Testing of retroviruses in HEK cell cultures, related to Figure 3.

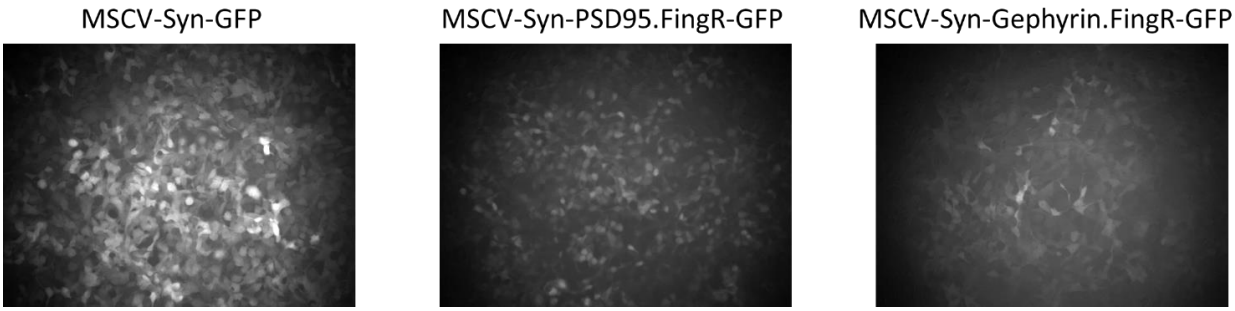

Retroviruses were tested in HEK cells. MSCV-Syn-GFP expression was the strongest (left), but MSCV-Syn-PSD95.FingR-GFP (middle) and MSCV-Syn-Gephyrin.FingR-GFP (right) showed reasonable but weaker expression. MSCV FingR viruses with transcriptional control did not show any fluorescence (data not shown).

Supplementary Figure 7. Validation of striatal cholinergic neuron labeling and 6OHDA induced dopaminergic terminal lesion, related to Figure 4.

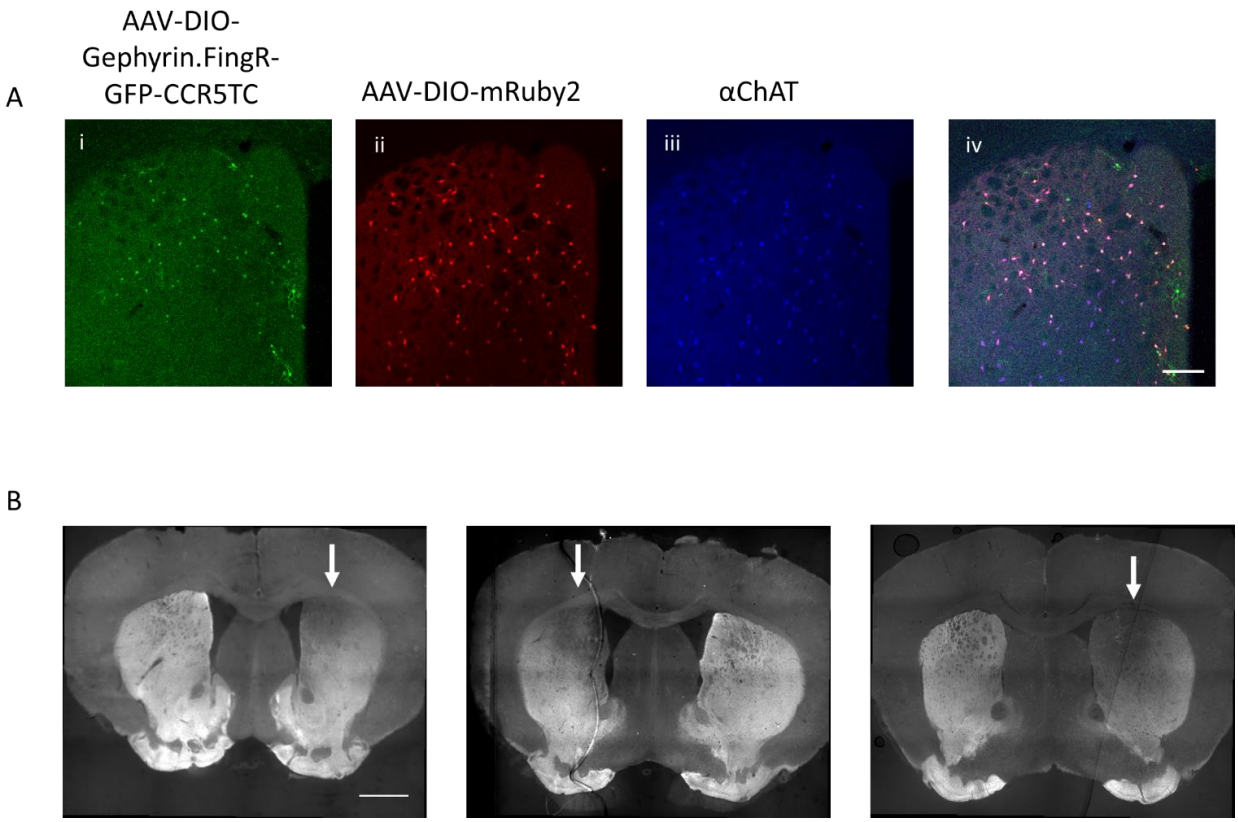

A) Neurons in ChAT-Cre mice co-infected with AAV-DIO-Gephyrin.FingR-GFP-CCR5TC (i) and AAV-DIO-mRuby2 (ii) were stained with a choline acetyltransferase antibody (iii) to confirm expression was restricted to cholinergic interneurons (iv). 91.5 +/- 4.5% (mean +/- standard deviation) of co-labeled cells were ChAT positive (n=4 mice). Scale bar 200um. B) Three representative brain slices with tyrosine hydroxylase staining showing dimmer staining on the lesioned hemisphere (indicated by white arrow). Scale bar 1mm.

Supplementary Figure 8. Quantification of distances between stained synaptic puncta, related to Figures 1 & 2 and Transparent Methods.

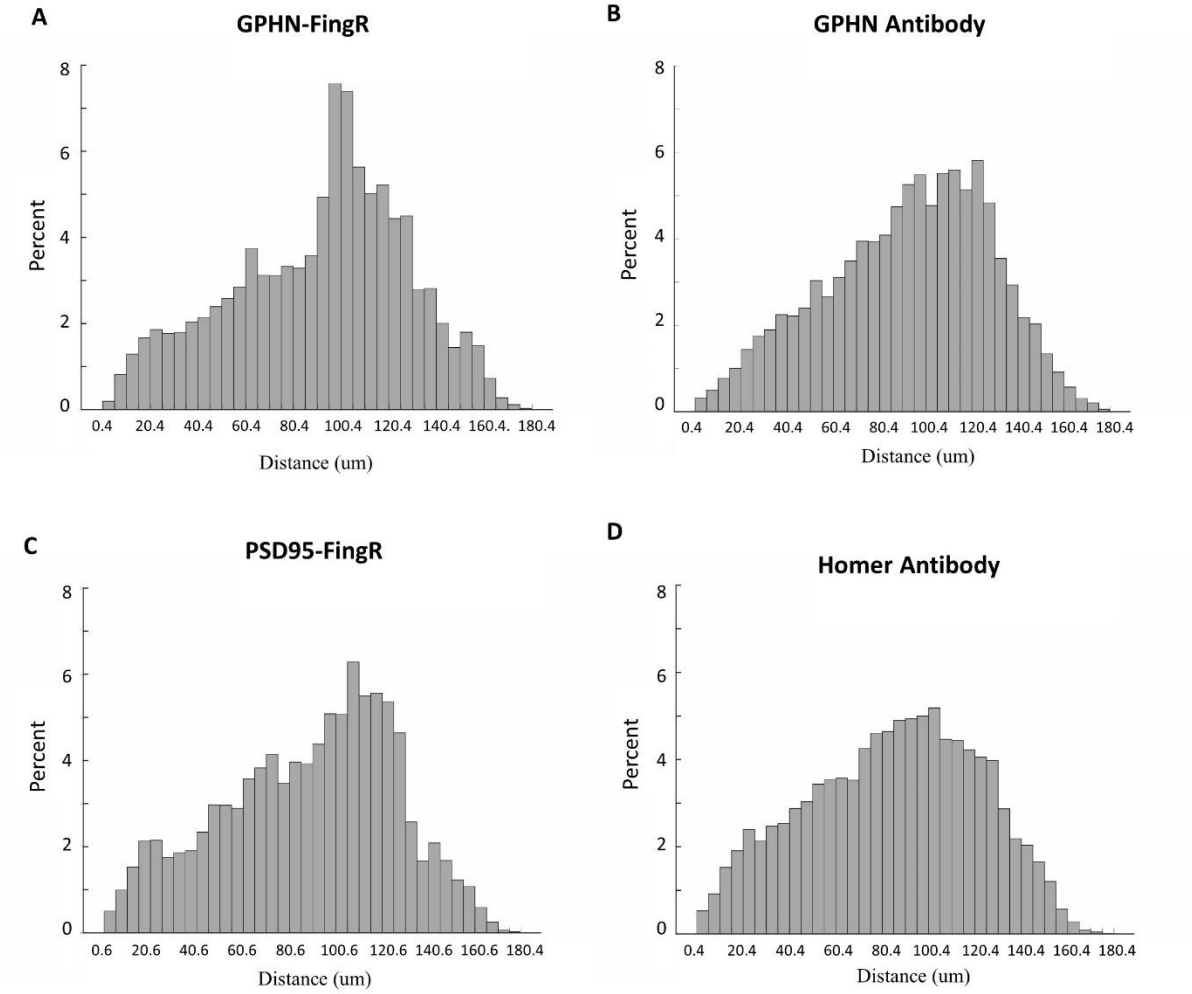

Distribution of the distance between puncta in mouse brain slices labelled with (A) AAV-mRuby2-Gephyrin.FingR-IL2RGTC; (B) GPHN antibody; (C) AAV-PSD95.FingR-GFP-CCR5TC, and (D) Homer antibody.

Transparent Methods

Molecular Cloning

The following plasmids served as the backbones for all viral genomic transfer plasmids: AAV-ReaChR-citrine (Addgene #50954) for AAV global synaptic labeling, pAAV-EF1A-DIO-mCherry-WPRE-pA (Addgene #37083) for cre-inducible AAV expression, and pMSCV-GFP (Addgene #86537) for retroviral labeling of adult born neurons. The EF1A promoter from the 8x2C mAGNET (Addgene #67955) was used for synaptic labeling. All other plasmids used the original EF1A or synapsin promoters from the backbones listed above. The PSD95.FingR, GPHN.FingR, GFP, and CCR5 or IL2RG transcriptional control regions were derived from pCAG-PSD95.FingR-GFP-CCR5TC (Addgene #46295) and pCAG-GPHN.FingR-mKate2-IL2RGTC (Addgene #42697). All DNA linker regions remained the same as in pCAG-PSD95.FingR-GFP-CCR5TC. The CCR5 or IL2RG transcriptional control DNA binding sites were inserted upstream of the promoter using custom DNA oligos (IDT DNA). Red fluorescent proteins and exogenous PSD95 were cloned from pmScarlet-i_C1 (Addgene #85044), pcDNA3-mRuby2 (Addgene #40260), or FU-dio-PSD95-mCherry (Addgene #73919). All plasmids were built using Gibson assembly or traditional cloning, and all plasmids will be available on Addgene for distribution.

AAV Production

AAV2 serotype 9 viral particles were packaged as described previously (Keaveney et al., 2018). Briefly, HEK293FT cells (R70007 Life Technologies) were triple transfected with an AAV genomic transfer plasmid, a pXX680 helper packaging plasmid, and a cap-9 plasmid coding for the Rep and Cap proteins to make AAV2 serotype 9 viral particles. After 72 hours, the cells were lysed and viral particles were collected from the cell media and lysed cells into a single tube. Viral particles were centrifuged to remove cell debris and the supernatant was filtered at 0.45µm. PEG-IT was added to the filtered viral supernatant and rotated at 4C overnight to precipitate viral particles out of solution. Supernatant was removed and AAV viral particles were re-suspended in PBS. All red Gephyrin.FingR AAVs were produced by the Janelia Virus Service Facility.

Retrovirus Production

All retrovirus was produced using methods as described previously (Zhuo et al., 2016). Briefly, HEK293FT cells (R70007 Life Technologies) were triple transfected with a MSCV retroviral vector expressing GFP, PSD95.FingR-GFP or GPHN.FingR-GFP under a synapsin promoter; pMD2.G which encodes the VSV-G pseudotyping coat protein (Addgene #12259); and the Gag/pol packaging plasmid (Addgene #14887). Viral particles were collected from the cell media, passed through a 0.45µm filter, and concentrated using ultracentrifugation. Supernatant was removed and viral particles were reconstituted in PBS.

Neuron Culture Preparation, Maintenance and Infection

Primary rat neuron cultures were prepared as described previously (Gilbert and Man, 2016). Briefly, brains were removed from embryonic day 18 pups, and dissociated neurons from the cortex and hippocampus were seeded onto glass coverslips coated in poly-l-lysine and cultured in supplemented neurobasal media. Fluorodeoxyuridine was added after one week to inhibit glial mitosis. Neuron cultures were infected between DIV7-DIV10 with 1-5ul of AAV per coverslip. Cells were imaged at least 3 days post infection to enable gene expression and ensure synapses had formed.

Animal Surgery and Handling

All animal procedures were reviewed and approved by the Boston University Institutional Animal Care and Use Committee. All stereotaxic viral or drug injections into the brain occurred while mice were anesthetized with isoflurane, using a 10µL syringe (NANOFIL, World Precision Instruments) fitted with a 33-gauge needle (World Precision Instruments, NF33BL) and controlled by a microinfusion pump (World Precision Instruments, UltraMicroPump3-4). The syringe was left in place for an additional 10 minutes to facilitate viral spread.

For global synaptic labeling, 2-6 month old, female C57BL/6 mice (Charles River Laboratories) were stereotaxically injected with 0.5-1ul of AAV, at a speed of 100nl/min, into the motor cortex (+1.8 AP, +/-1.5 ML, -1.0 Z), striatum (+0.7 AP, +/-1.8 ML, -2.45 Z), and CA1 region of hippocampus (-2.0 AP, +/-1.4 ML, -1.6 Z). 2 mice were injected per condition.

All retrovirally injected 8-10 weeks old adult C57BL/6 mice were housed with running wheels from one week before viral injection until they were sacrificed. 1.5ul of retrovirus was stereotaxically injected at a speed of 100nl/min into the dentate gyrus at sites: -2 AP, +1.5 ML, -1.9 Z and -2.8 AP, +2.0 ML, -2.0 Z. 3-4 mice were injected per condition.

For cre-dependent labeling and 6-OHDA experiments, male and female ChAT-cre mice (GM24Gsat, Mutant Mouse resource Center, Davis, CA), 2-6 months old, were stereotaxically injected with AAV-DIO-mRuby2/AAV-DIO-PSD95.FingR-GFP-CCR5TC or AAV-DIO-mRuby2/AAV-DIO-GPHN.FingR-GFP-CCR5TC. Viruses were mixed together at a 1:2 ratio (mRuby2:FingR) and 1.5ul of the viral cocktail was injected into each hemisphere of the striatum (+0.7 AP, +/-1.8 ML, -2.45 Z). One week later, mice were given an intraperitoneal injection of desipramine hydrochloride (10ml/kg) before stereotaxic injection of 1ul of freshly prepared 6-OHDA (6mg/ml, Sigma Aldrich) at a rate of 100nl/min into one hemisphere of the striatum (+0.7 AP, +1.8 ML, -2.45 Z). The 6-OHDA injection procedure was completed in the dark to prevent oxidation.

Immunocytochemistry

Neuron cultures were fixed for 10 minutes in a 4% paraformaldehyde and 4% sucrose solution and washed three times in PBS. Cell were incubated in 0.3% Triton for 10 minutes and blocked

in 10% goat serum for 30 minutes. Primary antibodies (PSD95 1:200, Neuromab 75-028; Gephyrin 1:300, Synaptic Systems 147011) were diluted in a 2.5% goat serum solution and incubated with the neurons overnight at 4C. Cells were washed three times in PBS, incubated with the secondary antibody diluted 1:500 in a 2.5% goat serum solution, washed three times in PBS, and then mounted for imaging.

Histology

All mice were perfused with PBS followed by 4% paraformaldehyde, and brains were post-fixed in 4% paraformaldehyde for 1-4 hours. Brains were cryoprotected in 30% sucrose at 4C, frozen, and sliced at 50µm on a cryostat for imaging or staining. The following primary and secondary antibodies were used: mouse anti-Gephyrin (1:200, Synaptic Systems 147011), rabbit anti-Homer (1:200, Synaptic Systems 160003), mouse anti-Bassoon (Abcam ab82958), goat anti-ChAT (1:500, EMD Millipore AB144P), or rabbit anti-Parvalbumin (1:1000, Swant Inc. PV27), followed by Alexa Fluor 568, Alexa Fluor 633, or Alexa Fluor 647 (1:200-1:1000, Life Technologies). During staining, slices were incubated in PTG buffer (PBS with 0.5% Triton X-100 and 100mM glycine) to quench spare formaldehyde for 30 minutes followed by blocking buffer (PBS with 0.5% Triton X-100 and 2% goat/donkey serum) for 2 hours. Primary antibodies were diluted at the specified concentrations in blocking buffer and incubated with slices overnight at 4C. Following washes with PTG buffer, secondary antibodies (1:200-1:1000) diluted in blocking buffer were added for 2 hours. Slices were washed with PTG buffer three times, incubated in PBS with 100mM glycine for 30 minutes, and subsequently mounted on glass slides for imaging.

Staining with tyrosine hydroxylase was performed using a similar protocol, but with Tris-HCl serving as the buffer. Tyrosine hydroxylase (Abcam Ab112) was diluted 1:750 and incubated with brain slices for 48 hours at 4C. The secondary antibody was used at a concentration of 1:200.

Image Acquisition

All images of synapses were taken using an Olympus FV1000 scanning confocal microscope, or the Olympus FV3000 scanning confocal microscope.

For global synaptic staining, images were collected using a 10x air and 60x water immersion objective. Fluorescence was excited with 470nm, 543nm and 633nm lasers, and collected with FITC, Rhodamine and CY5 filters for GFP/Alexa Fluor 488, Alexa Fluor 568 and Alexa Fluor 637nm fluorescence respectively. To visualize individual synapses, images were acquired with a 60x objective and additionally with a 4x magnification with the FV1000 confocal microscope, or 100x oil immersion objective with the FV3000 confocal microscope.

To image synaptic labeling in adult born neurons, one stack (z=4µm steps) was taken at 20x to identify viral expression in the dentate gyrus. For each slice, 1-2 FOVs were identified for quantification. Each FOV was imaged using a 60x water immersion objective at 2µm intervals. Further, at least 4 images were taken within each FOV using a 4x magnification for analyzing synaptic density along the dendrites at 0.53-0.57µm z-intervals. All images were acquired using a 470nm and 543nm laser for excitation and Alexa Fluor 488 and 568 emission filters. With unstained cells, the 568 emission filter was used to identify autofluorescence.

In 6-OHDA injected brain slices, stacks were acquired at 5µm intervals with a 10x objective in each hemisphere. Fluorescence was excited with 543nm and 633nm lasers and collected using Alexa Fluor 594 and Alexa Fluor 647 emission filters. Additional stacks were acquired at 60x magnification in 2µm step intervals and at 60x magnification with a 4x zoom in 1µm step intervals using 470nm, 543nm, and 633nm lasers with Alexa Fluor 488, 594, and 647 emission filters.

Tiled images to observe tyrosine hydroxylase staining were taken using a Nikon Eclipse fluorescence microscope. All slices were imaged with a 4x objective lens in the red and far red channels. Images were taken in a 4x4 grid centered in the middle of the brain slice. Additionally, 10x images were acquired on the Nikon Eclipse in the green, red, and far red channels for quantification of ChAT antibody and ChAT-cre virus co-localization.

Synaptic Density Quantification

To quantify synaptic density per dendritic length (Figures 3 J, K, and 4 H), we divided the number of synapses by dendrite length. To estimate dendrite length, a maximum intensity projection was taken of each image stack to measure dendrite length. Dendrites were traced and measured using the Neuron J plugin in Fiji (http://imagescience.org/meijering/software/neuronj/) (Schindelin et al., 2012).

Synapses in adult born neurons were analyzed using a custom Matlab program. Each image was passed through a Gaussian filter followed by background subtraction. The image was then sharpened and binarized. Connected components were selected as preliminary synapses and then filtered to identify regions of interest greater than $1\mu m^2$ to remove noise.

Synapses in cholinergic interneurons were manually selected. Synapse quantification was only performed in cells expressing both the mRuby2 cell marker and green FingR virus. Furthermore, only dendritic shafts that were clearly labeled by mRuby2 and expressed green puncta along the dendrite were used in quantification.

Co-localization analysis between synaptic puncta labelled with FingRs versus antibodies.

Synapse co-localization quantification was performed on brain slices from three mice injected with AAV-EF1A-GPHN.FingR-GFP-CCR5TC and three mice injected with AAV-EF1A-PSD95.FingR-GFP-CCR5TC. Synapses were identified using a custom Matlab program. Each image was first passed through a Gaussian filter with two dimensional Gaussian smoothing kernel using two standard deviations. The image was then binarized by setting all pixels with fluorescence intensity values smaller than the minimum intensity values of synapses to zero, and the rest of the pixels to 1. Connected components were selected as preliminary synaptic puncta, and then filtered to identify regions of interest greater than $1\mu m^2$ to remove noise.

Since the spatial resolution of our confocal microscopy is diffraction limited, we considered any two puncta within double the point-spread functions (0.4um) of the microscope as colocalized. We used a 60X objective lens with a NA of 1.4 for the FV1000 confocal microscope, and a 100X objective lens with a NA of 1.35 for the FV3000 confocal microscope. These objective lens have point spread functions of ~0.2 um for the 510nm-637nm light used for fluorescence imaging. As confirmed by **Supplementary Figure 8**, no two puncta in the same image were within two length of the point spread function.

Statistical Analysis

For synaptic integration of adult born granule cells, between group differences were analyzed by running a one-way ANOVA with a Bonferroni correction. The synaptic density in cholinergic interneurons with or without 6-OHDA lesioning were compared using a Wilcoxon Rank Sum test.

Supplemental References

Gilbert, J., Man, H., 2016. The X-Linked Autism Protein KIAA2022 / KIDLIA Regulates Neurite Outgrowth via N-Cadherin and δ -Catenin Signaling. eNeuro 3, 1–17.

Keaveney, M.K., Tseng, H. an, Ta, T.L., Gritton, H.J., Man, H.Y., Han, X., 2018. A MicroRNA-Based Gene-Targeting Tool for Virally Labeling Interneurons in the Rodent Cortex. Cell Rep. 24, 294–303.

Schindelin, J., Arganda-Carreras, I., Frise, E., Kaynig, V., Longair, M., Pietzsch, T., Preibisch, S., Rueden, C., Saalfeld, S., Schmid, B., Tinevez, J.Y., White, D.J., Hartenstein, V., Eliceiri, K., Tomancak, P., Cardona, A., 2012. Fiji: An open-source platform for biological-image analysis. Nat. Methods 9, 676–682.

Zhuo, J.M., Tseng, H.A., Desai, M., Bucklin, M.E., Mohammed, A.I., Robinson, N.T., Boyden, E.S., Rangel, L.M., Jasanoff, A.P., Gritton, H.J., Han, X., 2016. Young adult born neurons enhance hippocampal dependent performance via influences on bilateral networks. Elife 5.